UCLA-HEP-92-007

Lambda(c) and Sigma(c) Baryons Production in e^+e^- Annihilation at $\sqrt{s} = 29$ GeV

Sahak Khacheryan

June 1992

LOS ANGELES 90024
CALIFORNIA

UNIVERSITY OF CALIFORNIA

Los Angeles

Lambda(c) and Sigma(c) Baryons Production in e^+e^- Annihilation at $\sqrt{s} = 29$ GeV

A dissertation submitted in partial satisfaction of the requirements for the degree Doctor of Philosophy in Physics

by

Sahak Khacheryan

1992

The dissertation of Sahak Khacheryan is approved.

Francis Chen

Donald H. Stork

William Slater

Charles D. Buchanan, Committee Chair

University of California, Los Angeles

1992

DEDICATED TO MY PARENTS: LEVON AND ALIS KHACHERYAN

TABLE OF CONTENTS

LIST OF FIGURES

LIST OF TABLES

ACKNOWLEDGMENTS

While far from being a politician, I would like to express my gratitude and praise for the American educational system which gives equal opportunity to anyone from all over the world.

When the time comes for the expression of the awareness and the gratitude towards the ones who have contributed to this thesis then it is inevitable to make mistakes for not giving the proper regard to all participants. Within this multimillion High Energy experimental project, hundreds of dedicated scientists, engineers and technicians were involved for nearly three decades. Once again I would like to thank them all. Certainly there are some special senior scientists, colleagues and friends who have left a great impact on my academic achievements. I would like to express my gratitude to Mike Strauss and Hiro Yamamoto who always could spare precious time from their own research in order to provide helpful discussions with me and to give guidance in my early scientific career in High Energy Physics. It has been an honor for me to work with Al Eisner who is much admired for his genius scientific mind and depth of understanding. I have enjoyed knowing Mike Sullivan whose work ethic serves as a role model in the physics community. It has been an honor for me to work directly or indirectly with Donald Stork, Hans Sens, Hans Paar, Werner Hofmann, Mike Ronan, Gerry Lynch, Ed Miller, Ken Fairfield, Al Clark, Dick Kofler, Orin Dahl, Ron Ross, Dan Bauer, Elliott Bloom, Tony Barker, Dan Crane, Yao-Xun Wang. I would like to express special thanks to my field advisor Professor Charles Buchanan for his unstopping guidance, encouragement and inspiration. He has always been beside me whenever I was having crucial transitions in my scientific life. With

his charismatic personality he was able to create a healthy and enjoyable working environment within his research group which is so important for creative work.

There is another advantage to working within a large High Energy collaboration. Since there were quite a few graduate students within our collaboration who share similar interests and faith, then eventually we build friendship. I was fortunate enough to have James Yen-Tang Oyang, Mao-Tang Cheng, Sebong Chun, Rick Berg, Richard Belcinski, Alan Nicol as my colleagues and friends. I would like to say thanks to my male and female friends who did not let me become isolated from a nurturing social life.

I have reserved another special thanks for my parents: Levon and Alis Khacheryan. They were my primary educators and teachers at home, in my early school years, and in my everyday life. With my brother Gevorg and sisters Silvia and Arpine, we have always shared our happy and sad hours and occasions. My parents and my family members did their best to release me from everyday chores so that I could dedicate my time to study and research.

Thanks also to the Department of Energy for sponsoring this project.

VITA

1959	Born, Yerevan, Armenian Republic
1980	B.S. in Physics, Yerevan State University, Armenian Republic
1981-1983	Electronics Technician, Moore Ind., Los Angeles
1985	M.S. in Physics, University of California, Los Angeles
1984-1986	Teaching Assistant, Department of Physics University of California, Los Angeles
1985-1986	Research Assistant in Solid State Physics University of California, Los Angeles
1986-1992	Research Associate in High Energy Physics University of California, Los Angeles

PUBLICATIONS AND PRESENTATIONS

1. " The TPC/TWOGAMMA Cosmic Ray Detector", Mao-Tang Cheng, Sahak Khacheryan, and Hans C. Sens, TG-343, TOF-006 (1986).

2. " The Production of Λ_c Baryon in 29 GeV Electron-Positron Annihilation" (TPC/2γ Collaboration), paper presented by S. Khacheryan at the 1990 Spring Meeting of the American Physical Society, Washington, D.C.

---

3. " Inclusive D^{*+-} Production in Photon-Photon Collisions", H. Aihara et al., Phys. Lett. B252,499 (1990).

4. "Investigation of the Electromagnetic Structure of η and η' Meson by Two Photon Interactions", H. Aihara et al., Phys. Rev. Lett. 64,172, (1990).

5. "A Measurement of the Total Hadronic Cross-Section in Tagged Gamma-Gamma Reactions", H. Aihara et al., Phys. Rev. D41, 2667, (1990).

6. "Exclusive Production of $p\bar{p}\pi^+\pi^-$ in Photon-Photon Collisions", H. Aihara et al., Phys. Rev. D40, 2772, (1989).

7. "Evidence of Soft and Collinear Emission in e^+e^- Hadronic Events", H. Aihara et al., Z. Phys. C44, 357 (1989).

8. "f_1(1285) Formation in Photon-Photon Fusion Reactions", H. Aihara et al., Phys. Lett. B209, 107 (1988).

9. "Charged Hadron Inclusive Cross-Sections and Fractions in e^+e^- Annihilation at $\sqrt{s}$=29 GeV", H. Aihara et al., Phys. Rev. Lett. 61, 1263 (1988).

10. "Formation of Spin One Mesons by Photon-Photon Fusion", H. Aihara et al., Phys. Rev. D38, 1 (1988).

11. "Charmonium Production in Photon-Photon Collisions", H. Aihara et al., Phys. Rev. Lett. 60, 2355 (1988).

ABSTRACT OF THE DISSERTATION

Lambda(c) and Sigma(c) Baryons Production

in e^+e^- Annihilation at $\sqrt{s} = 29$ GeV

by

Sahak Khacheryan

Doctor of Philosophy in Physics

University of California, Los Angeles, 1992

Professor Charles D. Buchanan, Chair

Using the TPC/2γ detector at PEP, the Λ_c charmed baryon has been observed for the first time in e^+e^- annihilation at $\sqrt{s} = 29$ GeV via the $\Lambda_c \rightarrow PK\pi$ exclusive decay channel. The extracted Λ_c production rate per hadronic event is 0.12±0.05(stat) ±0.04(syst); the rate of Λ_c per c quark is 0.13±0.07(stat+syst). The Λ_c's also were searched for by looking at the $P\bar{K}^0$, $P\bar{K}^0\pi^+\pi^-$, $\Lambda\pi^+\pi^+\pi^-$, and Λe^+x hadronic and semileptonic decay channels; the estimated Λ_c multiplicity from each mode and its associated upper limit with 90% confidence is -.09±.09 <.15, .18±.30 <.70, .19±.15 <.31, and .14±.14 <.35, respectively. [The weighted average of the Λ_c multiplicity based on these five channels is 0.079±0.045(stat+syst).] There is an indication of a $\Sigma_c \rightarrow \Lambda_c\pi$ signal, where the ratio $(\Sigma_c^{++} + \Sigma_c^0)/\Lambda_c$ is 0.40±0.29 with an upper limit of <.74 (90% CL). Our analysis suggests, at the ~1.0-1.5 standard deviation level, that the branching fraction for $\Lambda_c \rightarrow PK\pi$ decay is larger than the currently accepted value of 4.3±1.1% and/or the Λ_c multiplicity is larger than the present predictions from hadronization models which cluster around ~0.04 to 0.055 multiplicity.

Chapter 1. Introduction

The Λ_c particle is the lowest mass charmed baryon. It is a composite particle containing a charm quark and an $(ud)_0$ spin=0 diquark. So far there are no strict theories which quantitatively describe the production mechanism of the Λ_c particle. This is because the present QCD (Quantum Chromo-dynamics) theory is nonperturbative in the hadron production processes where low-momentum-transfer kinematics is dominant. Because of this difficulty, models are developed which describe the hadronization process phenomenologically. For e^+e^- annihilations, the most successful models are those of LUND[1], WEBBER[2] and UCLA.[3] According to these models, the Λ_c particles are mainly created when an $(ud)_0$ diquark (produced from the QCD color field) combines with a primary charm quark produced in the e^+e^- annihilation. The rate of this hadron creation process per hadronic event (i.e., the "multiplicity") is highly model dependent. According to the LUND, WEBBER, and UCLA model predictions, the Λ_c multiplicity is .055, .043, and .04, respectively, at E_{cm}~29 GeV. This low production rate makes the Λ_c observation difficult. The new born Λ_c particle has a mean life time about 10^{-13} sec and decays through weak interactions. The possible decay forms of the Λ_c particles are semileptonic or hadronic decays. The branching fraction for any decay channel is not more than a few percent which makes the Λ_c observation even harder.

The study of the Λ_c particle is an important one since the experimentally estimated Λ_c production rate tests models such as WEBBER, LUND, and UCLA, which eventually may assist in the creation of a "calculable QCD" theory in the soft parton region. However, this is complicated by the fact that one measures the Λ_c production rate times the branching fraction of $\Lambda_c \to PK\pi$, where the latter is also difficult to measure. Thus this measurement may also shed light on the complicated and presently incalculable hadronic decay processes which involve nonperturbative QCD processes as well.

The historical background of the Λ_c particle prediction and its experimental observation is the following: in 1964 M. Gell-Mann[4] and G. Zweig[5] independently proposed three hypothetical particles (u, d, s quarks) as "building blocks" for the existing hadrons. Some leading theoreticians then started to speculate about the existence of a fourth "charm" quark. These speculations were mainly aesthetic and were based on the empirical observation that the quarks and leptons seemed to group into families (or generations). At that time four leptons and three quarks were known. The speculated fourth charm quark would make quark-lepton symmetry complete and would ensure the success of the Gauge theory in the Electro-Weak interactions. In 1974, the J/Ψ particle was observed independently by two different experimental groups, one at SLAC[6] and the second one at Brookhaven.[7] In the following two years, theoretical models were created which predicted the spectrum of the charmed hadrons and the values of their masses.[8] Among these hadrons was the Λ_c, the lowest mass charmed baryon. In 1975, the first evidence of a Λ_c event was observed in a neutrino-proton interaction experiment at Brookhaven National Laboratory.[9] In the next five years, the Λ_c baryon was observed in photon interactions[10] (Fermilab, 1976), proton-proton interactions[11] (ISR, CERN, 1979), and e^+e^- annihilation[12] (SPEAR(MARK II), SLAC, 1980, E_{cm}~5-8 GeV). The collaborations which have observed a Λ_c signal in e^+e^- annihilation via exclusive decay channels such as $PK\pi$ are: MARK II(SPEAR, E_{cm}=5.2 GeV), CLEO(10.5 GeV), and ARGUS(10.2 GeV). Though there is an indication of the Λ_c from MARK II at PEP(E_{cm}=29 GeV) via the semi-inclusive decay mode $\Lambda_c \to \Lambda\, e$ + missing ν, ours is the

first observation of the Λ_c in e^+e^- interactions at E_{cm}>10 GeV via an exclusive reconstructible decay channel.

In this analysis we have used the $e^+e^- \to$multihadron data collected by the TPC/2γ collaboration at PEP during December 1984 through March 1986. The total integrated luminosity was about 68 pb^{-1}. The main instrument in this experiment was the "Time Projection Chamber" (TPC) detector, a "second generation detector" which has efficient particle identification capability (based on the simultaneous measurements of the incoming particle's momentum and the ionization loss per unit length). This good particle identification made the Λ_c particle observation possible with our detector in our statistically limited data events, whereas previous detectors at E_{cm}~29 GeV could not see its exclusive decay modes. Though we examine other channels, we focus on the decay $\Lambda_c \to PK\pi$. Because we cannot separately measure the branching fraction $\Lambda_c \to PK\pi$, this experiment is restricted to measuring the Multiplicity*Branching-Fraction. By using the recent experimental branching fraction value, the Λ_c production rate per event (i.e., multiplicity) is estimated. This is compared with similar measurements made at E_{cm}~10 GeV. Attempts were also made to observe the Σ_c particles via their hadronic decay channel $\Sigma_c \to \Lambda_c \pi$. There is some indication of the signal which provides an upper limit on the fraction of Λ_c's originating from Σ_c's.

References

[1] B. Andersson, G. Gustafson, G. Ingelman and T. Sjöstrand, Phys. Rep. 97,31 (1983).

[2] B.R. Webber, Nucl. Phys. B238, 492 (1984).

[3] C. D. Buchanan and S. B. Chun, Phys. Rev. Lett. 59,1997 (1987).

[4] M. Gell-Mann, Phys. Lett. 8, 214 (1964).

[5] G. Zweig CERN Report 8419/TH 401(1964), Unpublished.

[6] G. S. Abrams et al., Phys. Rev. Lett., 33, 1452 (1974).

[7] J. J. Aubert et al., Phys. Rev. Lett., 33, 1404 (1974).

[8] A. De Rújula, H. Georgi, and S. L. Glashow, Phys. Rev. D 12,147 (1975);
M. K. Gaillard, B. W. Lee, and J. L. Rosner, Rev. Mod. Phys. 47, 277 (1975).

[9] E. G. Cazzoli et al., Phys. Rev. Lett., 34, 1125 (1975).

[10] B. Knapp et al., Phys. Rev. Lett. 37,882 (1976).

[11] D. Drijard et al., Phys. Lett. 85B, 452(1979);
K.L. Giboni et al., Phys. Lett. 85B,437(1979);
W. Lockman et al., Phys. Lett. 85B, 443 (1979).

[12] G.S. Abrams et al., Phys. Rev. Lett. 44, 10 (1980).

Chapter 2. Theory

In this project, charmed baryon production is studied as a product of e^+e^- annihilation. The e^+e^- annihilation and eventual $q\bar{q}$ creation may proceed either via electromagnetic (γ^*) interaction or via weak neutral current (Z^0) interaction (See Figure 2.1). Therefore, the amplitude squared for such process is $|A_\gamma + A_Z|^2$. The contribution of the interference term is about 10% of the pure electromagnetic process[1] for the center-of-mass energy of 29 GeV. The electromagnetic interaction total cross section up to order of $O(\alpha^2\alpha_s)$ is given by:[1]

$$\sigma(e^+e^-\longrightarrow\text{hadrons}) = \frac{4\pi\alpha^2}{S}\left(1+\frac{\alpha_s(Q^2)}{\pi}\right)\sum_q e_q^2 \qquad (2.1)$$

with
$$\alpha_s(Q^2) = \frac{12\pi}{(33-2n_f)\log(Q^2/\Lambda^2)} \qquad (2.2)$$

where S stands for the center-of-mass energy squared, α is electromagnetic coupling constant, e_q is the charge of the primary quark, $\alpha_s(Q^2)$ is QCD running coupling constant (it is called a running coupling constant because it is a continuous function of the center-of-mass energy squared Q^2), n_f is the number of the active quarks (and equals to 5 since $u\bar{u}$, $d\bar{d}$, $s\bar{s}$, $c\bar{c}$, and $b\bar{b}$ quarks can be created when Q=29 GeV), Λ is QCD parameter and must be determined from experiment (Λ ranges from 0.1 to 0.5 GeV and depends on n_f). The outgoing partons interact via the strong interaction color force and eventually convert into hadrons with 100% probability. This hadronization process is non-perturbative by its nature. This is because during the hadronization almost all partons are created out of the field or, more precisely, out of gluon decay with gluon invariant mass on order of few GeV where α_s can not be considered small. The created hadrons generally are unstable and they may decay into lighter and more stable hadrons or leptons. Only these relatively stable particles are able to reach the particle detectors and to be recorded. The general picture of these processes is illustrated in Figure 2.2. In this chain, if the particle decay branching ratios are known then it would be possible to study empirically the properties of the hadronization dynamics. Since the hadronization physics is not calculable (due to its non-perturbative nature) then there exist only models which describe the physical properties of the hadrons individually and as a whole. Nowadays there are two main schools of fragmentation models which have successfully survived. One is the string fragmentation school and the second one is the cluster school.

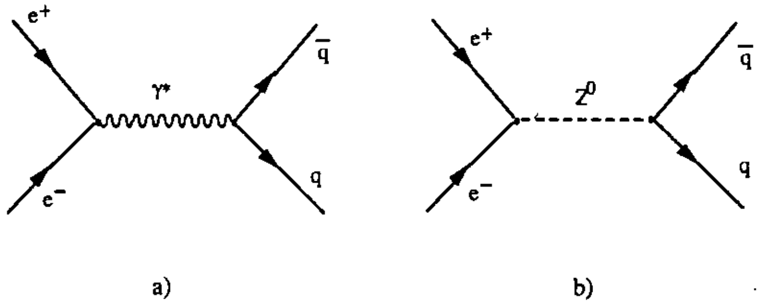

Figure 2.1 e+e- annihilation via a) electromagnetic or b) weak interaction.

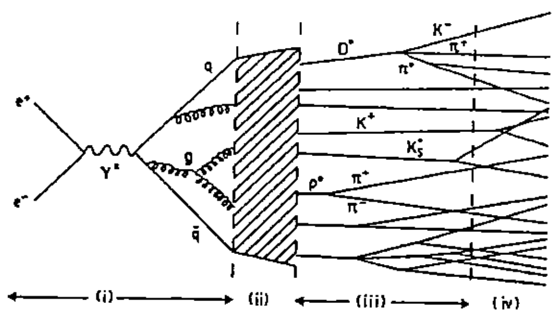

Figure 2.2 e+e- annihilation event with four significant phases: i) perturbative phase, ii) fragmentation phase, iii) relatively unstable particle decay phase, iv) detector observation phase.

2.1 String Fragmentation Model

One of the main characteristics of the strong interaction is that it is non-Abelian; i.e., the gluons - the carriers of the field - interact with each other. This interaction causes the strong interacting field between two quarks to be squeezed in transverse dimensions such that the color field can be approximated as a narrow cylindrical tube (See Figure 2.3). It is assumed that the transverse dimension of the tube is typically hadronic size, i.e., ~ 1 fm, and that the longitudinal size ranges from 1 to 5 fm before the colorfield tube starts to fragment. The next assumption is that the field flux is the same in any section along the tube. Therefore, the potential energy between the two departing quarks has a linear dependence on their separation distance. Consequently, the dynamics of the light quarks (like u, d, and s) within a quark pair system can be approximated by the dynamics of massless quarks connected through a massless relativistic string. The relativistic string has a string constant which is Lorentz invariant and, according to the heavy quarkonium spectroscopy, is about 1 GeV per fermi. It is presumed that the massless string stores the potential energy but no momentum and that the massless quarks carry the 4-momentum. The transverse excitation of the field tube and, consequently, for the string can be ignored. The substance of any string model is the adoption of the string concept and the formation of the hadrons by means of the string breakups, where the characteristic details may depend on the particular model under consideration. Since the uncertainty of the longitudinal momentum (due to Heisenberg uncertainty principle $\Delta p \Delta x \sim 1$) in general is much less than the absolute longitudinal momentum value (e.g., $\Delta p \sim .2$ GeV/c when $\Delta x \sim 1$Fermi=5.07 GeV^{-1}), then the dynamics in the longitudinal direction can be described semiclassically. The same thing is not applicable in the transverse dimensions and, therefore, the dynamics in this dimensions must be described quantum mechanically. The description of the longitudinal fragmentation processes can be restricted in 1+1 dimensions where one dimension is for the longitudinal dimension and the second one is for the time.

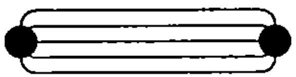

Figure 2.3 The $q\bar{q}$ color field with $V(r) \sim r$.

Nowadays the most dominant models among the string models are the LUND and UCLA models. These names are heritages of the universities' names where the string models were developed for several years.

2.1.1 LUND Model

The main characteristic of the LUND model[2,3] is that the fragmentation process highly depends on quark and diquark mass, spin, and flavor. It is presumed that the $q\bar{q}$ pairs continually create and annihilate inside the cylindrical field tube. When the separation between the quarks is large enough, then the field energy between the quarks would be able to support the transition of the intermediate virtual $q\bar{q}$ quark pair onto their mass shell. The mass shell of the quark is assumed to be its constituent mass. The constituent quark mass is the mass that, by means of the trivial quark mass summation in addition to the spin-spin interaction energy, makes up the hadronic mass. The newly created $q\bar{q}$ quark pair combine with the previously existing quarks and hadronize into colorless mesons and baryons. The dynamics of the quark pair creation and the formation of the hadrons in 1+1 (time and space) dimensions can be represented as in Figure 2.4. Here the $q_{i-1}\bar{q}_{i-1}$ pair is created at (x_{i-1},t_{i-1}) space-time coordinate and the $q_i\bar{q}_i$ pair is created at (x_i,t_i). The equation of motion for the i-th quark before it reaches the crossing point (the thick line shown on the Figure 2.4) is given:[4]

$$k(x-x_i) = \sqrt{P_o^2+m^2} - \sqrt{P^2+m^2} \quad \text{with} \quad P(t)=P_o - k(t-t_i) \qquad (2.3)$$

where P_o is the initial momentum of the i-th quark at $t=t_i$ and m is the quark mass. In the string model where the light quark masses can be ignored, the equation of the motion becomes $(x-x_i) = -(t-t_i)$ which describes a straight line in 1+1 dimensions. The hadron formation is assumed to take place when the world lines of the $q_i\bar{q}_{i-1}$ cross with each other. After the $q_i\bar{q}_{i-1}$ meeting, the potential energy of the string starts to increase at the expense of the quarks' kinetic energy until the quarks' trajectories reach their turning points. Consequently, the meson constituent quarks make a "yo-yo" type of motion. The i-th meson's ($q_i\bar{q}_{i-1}$ bound state) momentum and energy are given by:[5]

$$P_i = k(t_{i-1}-t_i), \qquad E_i = k(x_{i-1}-x_i). \qquad (2.4)$$

The enclosed area of the "yo-yo" type motion is a relativistic invariant and proportional to the meson mass squared:

$$\text{Area} = \frac{m^2}{2k^2} \quad . \qquad (2.5)$$

The creation times of the mesons with equal masses are ordered such that the less energetic meson is created first. This is based on the relativistic Lorentz time boost with the presumption that in the meson rest frame the meson formation takes about constant τ proper time. The $q\bar{q}$ creation is a quantum mechanical tunneling process, and the production probability per unit phase space in time and space is given by:[6,7,8]

$$d(\text{Probability})/dxdt \sim \exp(-\pi\, m_T^2/k) = \exp(-\pi\, m^2/k)\, \exp(-\pi\, P_T^2/k). \qquad (2.6)$$

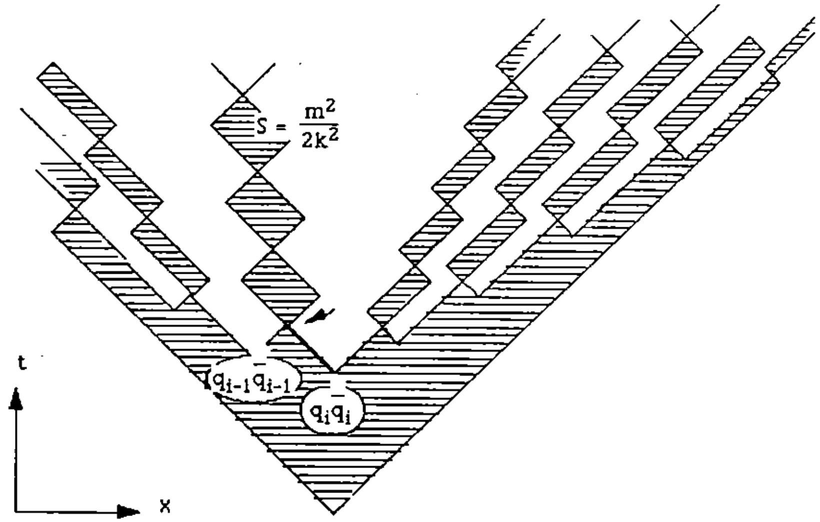

Figure 2.4 The dynamics of 1+1 dimensional string breaking and the formation of hadrons.

Here $m_T = \sqrt{m^2 + P_T^2}$ is the quark transverse mass which reflects the energy required to create the quark pair with quark mass m and transverse momentum P_T. Therefore, the P_T distribution is Gaussian with a width $<P_T>^2 = (350\ \text{Mev})^2$. In this estimation the transverse momentum broadening effect due to soft gluon radiation is also taken into account. The quark constituent masses have been used in order to estimate the quark production ratio u:d:s:c ~ 1:1:0.3:10^{-11}. Therefore, the production of heavy quarks, like charm and beyond, out of the colorfield can be ignored. The newly created quarks combine with the existing quarks and make vector or pseudoscalar mesons. The ratio of the vector meson probability over the pseudoscalar meson is controlled by two factors. One of them is the spin factor. Since the vector mesons are in a Spin=1 state, then they have three possible spin states, while the pseudoscalar mesons have only one. The second factor is the hadron mass factor. The heavier vector meson formation needs a larger string piece, i.e., larger phase space. Detailed calculations[9] show that, for mesons having the same quark content but different spin=0,1 states, then the meson production rate is roughly proportional to $1/m_{Meson}$. The phenomenological result for the ratio of the vector meson probability to the pseudoscalar meson probability is:

$$\frac{\text{Vector}}{\text{Pseudoscalar}} \sim \begin{cases} 1 & \text{For mesons containing u and/or d light quarks} \\ 1.5 & \text{For mesons containing one s quark} \\ 3 & \text{For mesons containing one charm or heavier quark} \end{cases}$$

Note that in the Vector/Pseudoscalar ratio the spin effect dominates for the mesons containing a charm or heavier quark.

A diquark concept has been used in describing baryon production. It has been assumed that the density of virtual $q\bar{q}$ pairs is so high that the probability to make a diquark out of the two virtual quarks is essentially equal to one; i.e., the diquark-antidiquark pairs can be considered as elementary particles. In this case the diquark suppression is controlled according to Formula 2.6 where m now is the diquark mass. The current algebra masses are used in order to determine the diquark mass differences for the different diquark flavor and spin configurations. The remaining one unknown diquark mass is $m(ud)_0$ and experimentally has been estimated from the overall Baryon/Meson ratio.

In addition to the baryon production by means of the diquark-antidiquark mechanism, the LUND model also implements the "popcorn mechanism" where there is a possibility to have a meson "popping out between baryon and antibaryon" (i.e., $BM\bar{B}$ configuration). Presently it is allowed to have only one meson popping out between the baryon and the antibaryon. The default value for the probability of the $BM\bar{B}$ configuration relative to overall $B\bar{B}$ and $BM\bar{B}$ configurations is equal to 50%.

The fragmentation process is a stochastic iterative process. The hadronic momentum distribution is derived by requiring that the characteristics of the fragmented hadrons must be independent of the starting point and of the direction of the fragmentation. This means that the fragmentation process must be "left-right" symmetric. Among the fragmentation functions which satisfy the "left-right" symmetry is :

$$f(z) = \frac{(1-z)^a}{z} \exp\left\{\frac{-bm_{TH}^2}{z}\right\} \qquad (2.7)$$

where $z = \frac{(E + P_L)_H}{(E + P_L)_q}$ is the fraction of the remaining jet energy-momentum carried by the outgoing hadron, $m_{TH}^2 = m_H^2 + P_{TH}^2$ is the known hadronic transverse mass squared where m_H is the hadron mass and P_{TH}^2 is chosen from the Gaussian distribution with $\sigma^2 = 2\langle P_T\rangle^2_{quark}$.

The contribution of hard gluon radiation is considered simply as a kink to the string and it is illustrated on Figure 2.5. The exact $O(\alpha_s)$ differential cross section for such a process is: .

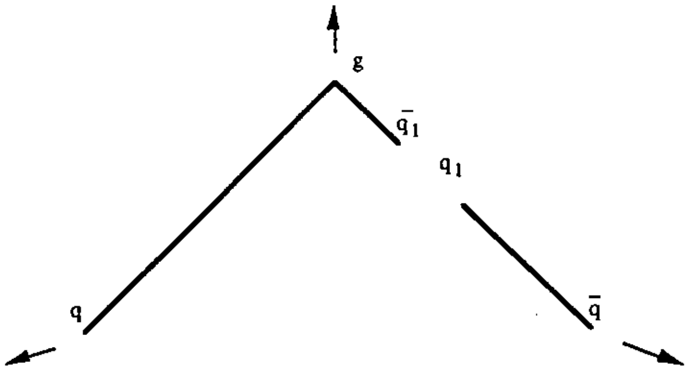

Figure 2.5 A hard gluon radiation gives a kink to the string.

$$\frac{1}{\sigma}\frac{d\sigma}{dx_1 dx_2} = \frac{2}{3}\frac{\alpha_s}{\pi}\frac{x_1^2 + x_2^2}{(1-x_1)(1-x_2)} \qquad (2.8)$$

where x_1, x_2 are scaled energy variables and $x_1 = \frac{2E_{q1}}{W}$, $x_2 = \frac{2E_{q2}}{W}$. The naive observation from Formula 2.8 suggests that the differential cross section turns into infinity for $x_1 \rightarrow 1$, or $x_2 \rightarrow 1$. But in reality the diverging terms are diminished by some interference terms between pure $ee \rightarrow q\bar{q}$ processes and $ee \rightarrow q\bar{q}$ processes including vertex and fermion QCD corrections. This argument is taken into account and the following requirement is enforced in order for an event to be qualified as a three jet event:

Parameter	Default value	Best tuned value
a	1.0	0.955
b	0.7	0.6
$\frac{s}{u}$	0.3	0.3
$\frac{qq}{q}$	0.1	0.1
$\frac{(us)/(ud)}{s/u}$	0.4	0.4
$\frac{1(qq)_1}{3(qq)_0}$	0.05	0.05
$\frac{\text{Vector meson}}{\text{all}}$ for u,d	0.5	0.5
$\frac{\text{Vector meson}}{\text{all}}$ for s	0.6	0.6
$\frac{\text{Vector meson}}{\text{all}}$ for c,b	0.75	0.75
popcorn	0.5	0.5
$\langle P_x \rangle_h = \langle P_y \rangle_h$	0.4	0.35

Table 2.1 The default and the best tuned parameter values for LUND Monte Carlo version 5.3.

$$m_{ij}^2 > y_{min} Q^2 \quad (2.9)$$

where m_{ij} is the invariant mass of any $q\bar{q}$, qg, $\bar{q}g$ pair and y_{min} is a constant parameter. A string stretches from the q to the g, then from the g to the $\bar{q}$. Since there are two strings connecting to the gluon, therefore, the gluon string constant equals to 2k. The fragmentation procedure of this three jet system is accomplished by transferring into the Lorentz frame where the piece of the linear string as a whole is at rest; then the fragmentation procedure is applied similarly to $q\bar{q}$ system. When the fragmentation processes terminate, then one more reverse Lorentz boost is applied which brings the system back to the original reference frame.

In conclusion, the LUND model is one of the most successful models and has about a dozen adjustable parameters. Mostly these adjustable parameters are on the quark level. The summary of the most significant parameters including their default and best data-tuned[10] values in LUND5.3 are listed in Table 2.1. In this thesis the LUND5.3 Monte Carlo program with its best tuned parameter values has been used extensively.

2.1.2 UCLA Model

The UCLA model[11,12,13,14] resembles both the string and cluster models. The UCLA suppression factors (like mass, spin etc.) are on the hadronic level, which is also the case for the cluster models (in particularly for the Webber model; see below), and the

scaled energy momentum (i.e., z) distribution of the hadrons in the UCLA model is controlled by the Lund Symmetric Fragmentation Function (LSFF) which is based on the relativistic string concept. The essential part of the UCLA model is that it interprets the Lund Symmetric Fragmentation Function with broader meaning than the LUND model does. In the UCLA model, it is expected that in any iteration step the LSFF gives, in addition to the distribution of the scaled energy and longitudinal momentum (as LUND does), the weight of the particular m_H hadron production rate among possible hadrons. Furthermore, the LSFF also gives hadronic transverse momentum distribution. It is worthwhile to emphasize that the LSFF, including a $(1-\frac{m_\perp^2}{\hat{s}z})$ correction factor (due to the limited value of the available center of the mass energy $(\hat{s})^{1/2}$) can be derived[15] from the Wilson Area Law[16] plus the available longitudinal momentum phase space. Besides sequential hadron production (where the flavor content of the hadron is shared by its preceding and following immediate neighbors), the UCLA model also presumes baryon production by means of the "popcorn" mechanism, where the mesons are produced between the baryon and anti-baryon pair. The hadron production weight depends on the following factors:

a) The available spin and flavor phase space determined by the Clebsh-Gordan coupling coefficients with the assumption that there is no spin correlation between the diquark and leftover anti-diquark.

b) The hadronic mass suppression determined by the LSFF.

c) The suppression of the heavy hadrons due to heaviness of the neighbor hadrons.

d) A "popcorn" production suppression of the form $\chi(\text{popcorn}) = \exp(-\eta M_p)$. In this expression M_p is the total mass of the "popcorn" mesons and the adjustable parameter η is ~ 2 Gev^{-1}. The "popcorn" suppression mechanism is still under study and needs more clarification concerning its principle basis and implications.

In order to preserve transverse momentum, the UCLA model requires, in the outside-in iteration implication, that the P_T distribution of each following hadron be centered at $(-\frac{P_T^{T\alpha}}{2})$ with a distribution function $\exp\left\{-b\frac{2P_{TH}^2}{z}\right\}$. This is an approximation to the case when the P_T value for a particular hadron is statistically compensated by the two hadrons for its immediate left and right. In overall, the hadron production probability density in a particular step is

$$P(m_H, z, P_{TH}^2) = N\frac{(1-z)^a}{z}\exp\left\{\frac{-b(m_H^2+2P_{TH}^2)}{z}\right\}\left\{1-\frac{m_H^2}{\Lambda s z}\right\}^a \cdot \mathrm{Clebsh\_Gordan}^2 \cdot \chi(\mathrm{popcorn}) \tag{2.10}$$

where a and b are adjustable parameters and N is a universal constant. The final weight of each candidate hadron is determined by its own weight (see equation 2.10) and also by the weight originating from the following three iterations. In particularly, heavy mass production is suppressed by its neighbor hadrons, because the leftover heavy quark (s) or diquark (ud,...) becomes part of another following heavy hadron.

In conclusion, the UCLA model has four adjustable parameters and two choices. The Λ adjustable parameter controls the parton shower and determines the kinks on the string; a and b are adjustable parameters which are part of the LSFF; and η parameter controls the "popcorn" suppression. One of the choices is that of local transverse momentum compensation (described above); the second choice is that the leftover quark or diquark has a fully free spin space for its magnitude and for its projections as well.

The remarkable thing about UCLA model is that it describes the property of the hadronization physics as well as LUND model does while having many fewer adjustable parameters. The UCLA model, due to its rigidity, is a powerful model in respect to its higher predictive ability comparing to LUND model.

2.2 Cluster Fragmentation Model

Cluster models are based on the parton shower phenomenon and on the formation of colorless clusters by means of combining the partons located nearby in coordinate and momentum space. The formed clusters may decay either into two lighter clusters or into hadron resonances and observable hadrons. The details of the cluster formation depend on the particular fragmentation models.

WEBBER Model[17,18,19]

The heart of any cluster model is the parton shower process.[20] In the Webber model the parton shower always is evaluated in the perturbative leading-log approximation, while being aware that its validity in the lower parton invariant mass region (where $\alpha_s(Q^2)$ is not small) is questionable. As a result of the e^+e^- annihilation, an outgoing $q\bar{q}$ pair is created which emit gluons. The gluons by themselves may branch into either gg or $q\bar{q}$ pair and so on (See Figure 2.6). Consequently, the parton shower takes place where the mass virtualities of the daughter partons are much smaller than the mass virtuality of the parent parton. The probability for the branching process $a\rightarrow bc$ (where the $a\rightarrow bc$ process represents any of these $q\rightarrow qg$, $g\rightarrow gg$, $g\rightarrow q\bar{q}$) is given by the Altarelli-Parisi evolution equation:

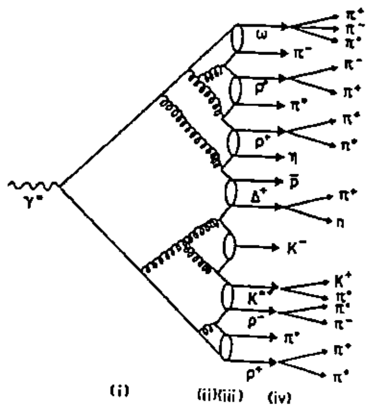

Figure 2.6 Schematic diagram for an e+e- annihilation event with cluster fragmentation. The four phases are shown: i)showers evolution, ii)forced $g\rightarrow q\bar{q}$ decay, iii)cluster formation, iv)cluster decay.

$$\frac{dP_{a\rightarrow bc}}{d(\log m_a^2)} = \int_{z_{min}}^{z_{max}} dz \, \frac{\alpha_s(P_T^2/\Lambda^2)}{2\pi} P_{a\rightarrow bc}(z) \qquad (2.11)$$

where α_s is the running coupling constant. If higher order loop corrections are taken into account properly, then α_s in reality, is a function of the relative transverse momentum of the outgoing partons $P_T^2 = z(1-z)m_a^2$ (instead of Q^2 (or m_a^2)), where z is a fraction of the energy carried by one of the daughter particles. $P_{a\rightarrow bc}(z)$ is the Altarelli-Parisi splitting function which defines the energy splitting between two outgoing quarks and is given by:

$$P_{q\rightarrow qg}(z) = \frac{4}{3}\frac{1+z^2}{1-z} \qquad (2.12)$$

$$P_{g\rightarrow gg}(z) = \frac{6(1-z(1-z))^2}{z(1-z)}$$

$$P_{g\rightarrow q\bar{q}}(z) = \frac{1}{2}(z^2+(1-z)^2).$$

The selection of the daughter parton virtuality is done using Sudakov form factors:

$$S_{a\rightarrow bc}(m^2) = \exp\left\{ - \int_{m_{min}^2}^{m^2} \frac{dm'^2}{m'^2} \int_{z_{min}(m')}^{z_{max}(m')} \frac{\alpha_s(P_T^2/\Lambda^2)}{2\pi} dz \, P_{a\rightarrow bc}(z) \right\} \qquad (2.13)$$

where $S_{a\rightarrow bc}(m^2)$ is the probability that the daughter parton does not have mass virtuality within the region m_{min} to m. This definition is based on the assumption that the statistics of the emission process obeys a Poisson distribution with the mean value expressed by the form inside the parentheses of the Equation 2.13 with positive sign. From the definition of the Sudakov form factor, it follows that the probability of the parton to have a virtuality in the region of the m^2 and $(m+dm)^2$ is:

$$P_{a\to bc}(m^2)\,dm^2 = \frac{d}{dm^2}\left\{\frac{S_{a\to bc}(m^2_{max})}{S_{a\to bc}(m^2)}\right\}dm^2 \quad . \tag{2.14}$$

In the case of the soft or low energy gluon, where the wavelength of the newly created gluon is relatively large, the gluon formation can not be considered independent from the rest of the system. This coherence effect can be estimated from the destructive interference phenomenon between the Feynman diagrams in the leading log approximation. The overall effect of this destructive interference is that the opening angles are ordered in the decreasing order for the consecutive shower decays, i.e., $\theta_b<\theta_a$, $\theta_c<\theta_a$, where θ_a, θ_b, θ_c are the opening angles when the parent particles were a, b, and c, respectively. The proper usage of this coherence effect regulates the excessive soft gluon emission. It is interesting to observe that for the hard decay processes the angular ordering exists as well. Since the integrand in the Sudakov form-factor (See Equation 2.13) has a mass singularity, it then follows that the daughter partons' mass virtualities in generally are much smaller than the mass virtuality of the parent parton (i.e., $m_b^2, m_c^2 \ll m_a^2$). So the asymptotic form of the parent invariant-mass-squared reads $m_a^2 = m_b^2 + m_c^2 + 2E_bE_c\zeta \approx 2z(1-z)E_a^2\zeta$, where $E_b=zE_a$, $E_c=(1-z)E_a$, $\zeta = \frac{P_b \cdot P_c}{E_bE_c}$ (and in the case when the parton mass virtuality is much less than its energy then $\zeta\approx(1-\cos\theta_a)$ where θ_a is the opening angle between two daughter particles). Therefore, for the hard decay processes, where z is far from the 0 or 1 limits, the $2z(1-z)E_a^2$ coefficient for two consecutive decays can be considered as the same order. Consequently, from the strong ordering of the virtual masses it follows that the opening angles are ordered too. More convenient evolution variable is chosen in order to describe the hard and soft parton shower processes. A new variables set $(z,\ t=\frac{E^2\zeta}{\Lambda^2})$ is chosen instead of $(z,\ m^2)$ for the Equations 2.13, and 2.14, where E is the parent energy

and ζ is defined as above. It is worth noticing that the Jacobian for the transformation from the old variables z, $\log(m^2)$ to the new variables z, $\log(t)$ is equal to one. The parton shower is generated in the boosted reference frame where each initial parton (the ones which result from the virtual photon decay) has energy $E_a=\frac{E_{cm}}{\sqrt{2}}$ or, equivalently, the opening angle between the initial partons is $\theta_0 = 90^0$ (i.e., $\zeta_0=1$). From Equation 2.14 (where the m^2 is replaced by the $t=\frac{E^2\zeta}{\Lambda^2}$), t is selected. Then, since E_a is known, the ζ_a is found from $t = \frac{E_a^2\zeta_a}{\Lambda^2}$. Then the z value is generated within the range (z_{min}, z_{max}) from the Altarelli-Parisi splitting function $P_{a\to bc}(z)$. After this, the daughter particles' energies are found: $E_b=zE_a$, $E_c=(1-z)E_a$. Then the next parton shower stage starts, where the b and c partons decay. In these cases the angular ordering conditions must be imposed (i.e., $\zeta_b\leq\zeta_a$, $\zeta_c\leq\zeta_a$) which practically have an effect only on the soft parton decay processes. A "fictious mass" has been adopted in this model for the gluon with m_g=.6 GeV. The constituent quark mass values are used for the u, d, s, c, b quarks where $m_d=m_u$=.3 GeV, m_s=.5 GeV, m_c=1.5 GeV, and m_b=5 GeV. The shower processes stop if $\zeta < \zeta_{min}=\frac{(Q_b+Q_c)^2}{E_a^2}$.

In this expression, Q_b represents the quark mass if b is a quark (with five possible flavor choices u, d, s, c, b), and Q_b represents the gluon mass if b is a gluon. The remaining gluons in the final stage of the parton shower are forced to decay into $u\bar{u}$ and $d\bar{d}$ pairs. After the parton shower termination, the partons' on-shell mass values are ascribed to the final emerging partons. The mother's invariant-mass is reconstructed by moving from the daughters to the mothers and using the exact formula $m_a^2 = m_b^2 + m_c^2 + 2z(1-z)E_a^2\zeta$. By knowing the partons' energies, transverse momenta (relative to the parent momentum direction; $P_T=z(1-z)m_a^2$), mass values and by randomly choosing the azimuthal angle, it is straightforward to reconstruct the partons' four-momenta. When the partons' four-momenta reconstruction is complete, the system is boosted back to the original reference frame where the initial partons were oriented back to back.

The hadronization phase proceeds as the parton shower terminates. Only the final stage partons (i.e., quarks) are involved in this hadronization phase. A quark and antiquark which are nearby in coordinate and momentum phase space combine into a colorless cluster. The colorless cluster concept is more mathematical than physical since continuous mass, but no spin (the model is ignorant about the cluster spin), is attributed to clusters. If the cluster mass is less than the "fission" mass (which is chosen to be Q_f~4 GeV) then the cluster decays isotropically into hadrons with weight factors equal to the product of the available spin space and momentum phase space. For example, if initially there was a $q_1\bar{q}_2$ cluster with mass <4 Gev then a $q_3\bar{q}_3$ pair is generated were q_3 could be a quark or an anti-diquark and it could be one of these choices: u, d, s, c, $\overline{uu}$, $\overline{ud}$, $\overline{us}$, $\overline{dd}$, $\overline{ds}$, $\overline{ss}$. The hadron candidate is expected to be one of the states 0^-(pseudoscalar), 1^+(pseudovector), 1^-(vector) and 2^+(tensor) if it is a meson, and one of the states $\frac{1}{2}^+$("octet"), $\frac{3}{2}^+$("decuplet") if it is a baryon. The production rate of these hadrons is controlled by a weight factor equal to $(2S_1+1)(2S_2+1)\frac{2p}{m}$ where S_1 and S_2 are the spins of the two product hadrons and p is the common momentum of the daughter clusters in the rest frame of the parent particle with mass m. Consequently, the hadrons are created with discrete spin and mass values. The remnant energy-momentum is transferred to the nearby cluster in order to preserve energy and momentum conservation.

When the cluster has comparably large mass (mass > 4 GeV) then the isotropic decay mechanism must be abandoned. In this case the constituent partons inside the cluster have comparably large kinetic energy. Therefore, the product cluster in the rest frame is expected to have momentum approaching the constituent parton momentum direction (See

Figure 2.7). Since there are not many clusters with mass larger than 4 GeV (they make up about 10%), then the selection of the heavy cluster particular fragmentation mechanism is not so crucial. In the standard Webber model the "symmetric string breaking" scheme has been adopted with the presumption that during the cluster breakup only the $d\bar{d}$, $u\bar{u}$, $s\bar{s}$ quark pairs (and no diquark pairs) are created with equal probability. According to this scheme, if P^μ_A and P^μ_B are four momenta of the product clusters then they are equal to:

$$P^\mu_A = \left(1 - \frac{Q_0}{M_c}\right)P^\mu_1 + \frac{Q_0}{M_c}P^\mu_2 \quad \text{and} \quad P^\mu_B = \left(1 - \frac{Q_0}{M_c}\right)P^\mu_2 + \frac{Q_0}{M_c}P^\mu_1 \, . \tag{2.15}$$

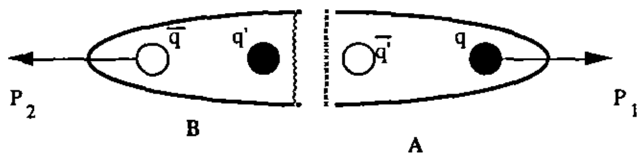

Figure 2.7 The heavy cluster decay is displayed.

If the newly created cluster has mass larger than Q_f, the above mentioned heavy cluster fragmentation procedure repeats once more. Whenever the product cluster's mass is less than Q_f, then the isotropic "fission" decay proceeds.

In order to accommodate the baryon production rate as indicated by data, it is presumed that a gluon can decay into diquark-antidiquark pair. When the virtuality of the parent gluon is less than Q_d, the gluon decay into diquark-antidiquark pair process is turned on. In this model uu, ud, dd diquarks are produced with equal probability and their production intensity is proportional to $\mathrm{Log}Q^2$. To provide appropriate baryon rates, the ratio of the overall diquark-antidiquark pair production rate to the quark-antiquark production rate needs to be .05.

The Webber model must be modified for the heavy hadron creation case when the newly produced hadron contains at least one charm or heavier quark. This is because the spectroscopy of the heavy flavor resonance multiplets so far is underdeveloped. In this case if the original cluster contains a heavy quark (charm quark or heavier quark) then the adopted cluster decay mechanism is not applicable and the heavy quark is allowed to decay via the weak interaction.

In summary, the Webber model has four major parameters: 1) Λ =.25 parameter which is the argument for the running coupling constant α_s, 2) m_g=.6 GeV fictious gluon mass, 3) M_f=4 GeV fission threshold, 4) Q_d gluon virtuality threshold below which the gluon decay into diquark-antidiquark pair is allowed. In addition to these, the model depends on the constituent quark mass values:

$$m_u=m_d=.3\text{ GeV},\quad m_s=.5\text{ GeV},\quad m_c=1.5\text{ GeV},\quad m_b=5.0\text{ GeV}.$$

2.3 Λ_c Production Mechanism and Models

The hadron production mechanism in the string models may proceed directly or indirectly. In the direct mechanism the hadrons are made by quarks or diquarks which are the products of the initial virtual photon decay and color field conversion. In the indirect hadron production case, the hadrons are the debris of the decays of another higher mass hadron.

In the LUND model the direct Λ_c's ($\bar{\Lambda}_c$'s) are produced when the created diquark $(ud)_0$ ($(\overline{ud})_0$) combines with the primary c ($\bar{c}$) quark. There are two main indirect Λ_c production mechanisms which make a significant contribution to the overall Λ_c production rate. One of these contributions originates from the Σ_c^{++}, Σ_c^{+}, Σ_c^{0} and Σ_c^{*++}, Σ_c^{*+}, Σ_c^{*0} particles when they decay into $\Lambda_c\pi$ via strong interactions with 100% branching fraction. The $b\bar{b}$ events are the second indirect Λ_c production source, when the hadrons containing the b quark may decay into Λ_c and some other debris. The fraction of the total Λ_c's production rate from these channels are about 50% and 16%, respectively.

In the UCLA model, the Λ_c production mechanism is principally similar to LUND model except that the production rate is regulated by the hadron level suppression factors.

In the WEBBER model, the Λ_c's are mainly produced when the cluster containing a charm quark in it decays into a Λ_c and another baryon. This cluster decay rate is determined by the available spin and momentum phase space. Besides this direct Λ_c production mechanism, there are Λ_c contributions originating from the Σ_c particles and $b\bar{b}$ events as well.

The present LUND, UCLA and WEBBER model predictions for the Λ_c production rate per hadronic event at E_{cm}=29 GeV are .055, .040, and .043, respectively. In these models the Λ_c production rate is expected to be relatively stable and independent of E_{cm}. The Λ_c's, unlike to light hadrons, are produced within a few clear-cut hadronization steps, and the Λ_c's properties, particularly the multiplicity value, reflect the conceptual design of the particular model in interest.

2.4 Λ_c Branching Fractions

The Λ_c is a composite particle whose constituents are u, d, and c valence quarks. It is the ground state energy level of charmed baryons. The spin and isospin values for the Λ_c particle are 1/2 and 0 respectively. It is possible to reconstruct the spin×flavor wavefunction of the Λ_c particle by using the orthogonality relationships of the Λ_c flavor wavefunction relative to completely symmetric and antisymmetric "udc" flavor wavefunctions. The Λ_c spin×flavor wavefunction is given by:[21]

$$\Lambda_c\uparrow = \frac{1}{\sqrt{12}}(u\uparrow d\downarrow c\uparrow - u\downarrow d\uparrow c\uparrow - d\uparrow u\downarrow c\uparrow + d\downarrow u\uparrow c\uparrow + d\downarrow c\uparrow u\uparrow - d\uparrow c\uparrow u\downarrow - u\downarrow c\uparrow d\uparrow + u\uparrow c\uparrow d\downarrow + c\uparrow u\uparrow d\downarrow - c\uparrow u\downarrow d\uparrow - c\uparrow d\uparrow u\downarrow + c\uparrow d\downarrow u\uparrow).$$

In the above wavefunction, if (ud) is considered as a two particle system then it can be concluded that (ud) is in spin=0. This is because the Λ_c wavefunction changes the sign under the spin exchange of the u, d quarks. It is evident that the (ud) system is in isospin=0

state since the remaining c valence quark does not carry isospin and does not contribute to overall the Λ_c isospin.

The Λ_c particle decay is an area of considerable interest. Since energy conservation does not allow Λ_c decay via strong interactions and since there is no open channel for the electromagnetic decays, then the only possibility for Λ_c decay is via weak interactions via either semileptonic or hadronic decay channels. The interesting point is that during the hadronic decay the strong interactions are also involved. The semileptonic decay is comparably simpler and it is calculable.

2.4.1 Λ_c Semileptonic Decay[22,23]

The semileptonic decay is illustrated in Figure 2.8 where l^+ can be interpreted as e^+ or μ^+. The following analyses[24] apply for both $\Lambda_c \rightarrow \Lambda e^+ \nu$ and $\Lambda_c \rightarrow \Lambda \mu^+ \nu$ decays. The decay process is examined in the spectator quark approximation where the (ud) quarks participate as spectators and the charm quark decays as a free particle. In this analysis care has been taken so that the $\Lambda_c \rightarrow \Lambda l^+ \nu$ decay rate dependence on the quark mass values is minimal. The decay rate expression will be expressed in terms of the observable parent and daughter hadronic masses. In this sense the (ud) quarks are not merely spectators. The standard form for the decay rate in terms of the amplitude and available phase space is:

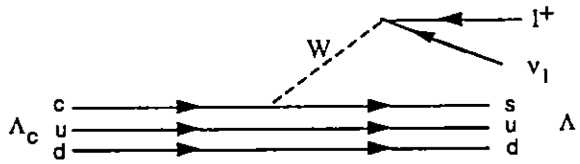

Figure 2.8 Λ_c semileptonic decay (ud spectator model).

$$d\Gamma(\Lambda_c \to \Lambda e^+ \nu) = \frac{1}{2M_{\Lambda_c}} \left| A(\Lambda_c \to \Lambda e^+ \nu) \right|^2 d\Pi_3 \qquad (2.16)$$

where $d\Pi_3$ is the momentum phase space factor for three Λ, e^+ and ν particles. $d\Pi_3$ factor is given:

$$d\Pi_3 = (2\pi)^4 \delta^{(4)}(P-k-p-p') \prod_f \frac{d^3k_f}{(2\pi)^3 2E_f} \qquad (2.17)$$

where P is the Λ_c four-momentum and k, p, p' are four-momenta of the final product Λ, e^+ and ν particles, respectively. The decay amplitude has the form of the weak current-current product form and it is given by:

$$A(\Lambda_c \to \Lambda e^+ \nu) = \frac{G_F}{\sqrt{2}} V_{cs} L^\mu H_\mu^{s's} \qquad (2.18)$$

where V_{cs} is the Kobayashi-Maskawa matrix element, L^μ is the leptonic current and $H_\mu^{s's}$ is the hadronic current when the parent and the daughter have s and s' spins, respectively. According to general rules, the L^μ and $H_\mu^{s's}$ have the form:

$$L^\mu = \bar{u}_e \gamma^\mu (1-\gamma_5) v_\nu \quad \text{and} \quad H^{(s's)\mu} = <k,s'|V^\mu - A^\mu|P,s>. \qquad (2.19)$$

The hadronic vector current can be reconstructed out of all available independent four-vectors γ^μ, $(p+k)^\mu$, $(p-k)^\mu$ with proper Lorentz invariant coefficients. Therefore, the parametrized hadronic vector current reads:

$$<k,s'|V^\mu|P,s> = \bar{u}_m(k,s')[g(q^2)\gamma^\mu + g_+(q^2)(p+k)^\mu + g_-(q^2)(p-k)^\mu] u_M(P,s) \,. \qquad (2.20)$$

Similarly, the hadronic axial current reads:

$$<k,s'|A^\mu|P,s> = \bar{u}_m(k,s')[a(q^2)\gamma^\mu\gamma_5 + a_+(q^2)(p+k)^\mu\gamma_5 + a_-(q^2)(p-k)^\mu\gamma_5] u_M(P,s) \qquad (2.21)$$

where $q^2 = (P-k)^2$. After some integration the differential rate reads:

$$\frac{d\Gamma}{dy} = \frac{G_F^2 |V_{cs}|^2 K M^2 y}{96\pi^3} (|H_+|^2 + |H_-|^2 + |H_0|^2) \qquad (2.22)$$

where $y = q^2/M^2$;

$$K \equiv \frac{M}{2}\left[\left(1 - \frac{m^2}{M^2} - y\right)^2 - 4\frac{m^2}{M^2} y\right]^{1/2} ; \qquad (2.23)$$

$$H_{\pm} \equiv \pm\, [aF_0 + gF_-]\,; \tag{2.24}$$

$$H_0 \equiv \left\{\left[2a\left(1 - \frac{1}{2}F_0\right) - 2ka_+F_-\right]^2 + (2kg_+F_0 + gF_+)^2\right\}^{1/2}; \tag{2.25}$$

$$F_{\pm} \equiv \left[\frac{(E_m + m)(E_M + M)}{4Mm}\right]^{1/2}\left[\frac{k}{E_m + m} \pm \frac{k}{E_M + M}\right]; \tag{2.26}$$

$$F_0 \equiv \left[\frac{(E_m + m)(E_M + M)}{4Mm}\right]^{1/2}\left[1 - \frac{k^2}{(E_m + m)(E_M + M)}\right]. \tag{2.27}$$

Here M and m are the Λ_c and daughter Λ baryon masses, respectively, and $k=\frac{K}{\sqrt{y}}$ is the momentum of the daughter Λ baryon in the frame where $e^+\nu$ is at rest.

In order to estimate the Lorentz invariant form factors, a comparison is done between the quark-model current and parametrized current. In Table 2.2, the form factors are listed which are evaluated at the maximum q^2 (where the daughter particle is at rest in the parent's rest frame). According to the "pole dominance model", the extended behavior of the form factors is:

$$\text{Form\_Factor}(y) = \frac{y_{max} - y_{res}}{y - y_{res}} * \overline{\text{Form\_factor}} \tag{2.28}$$

where $\overline{\text{Form\_factor}}$ is any of these coefficients a, a_+, a_-, g, g_+, g_- evaluated at maximum q^2, $y_{max} = (1-m/M)^2$, $y_{res} = (m^*_{sc}/M)^2$ and m^*_{sc} is the mass of the first cs vector-meson resonance which is above the parent baryon mass.

m_s (Gev)	m^*_{sc} (Gev)	V_{Qq}	$\bar{a}_+=\bar{a}_-$	$\bar{g}$ (Gev)	$\bar{a}$ (Gev)	$\bar{g}_+=\bar{g}_-$	$\Gamma(\Lambda e^+\nu)$ $10^{10}s^{-1}$	Γ_{Tot} (Exp) $10^{10}s^{-1}$	BF(%) $(\Lambda e^+\nu)$
0.51	2.5	.975	-.48	4.0	1.8	-.48	9.8	523	1.9

Table 2.2 The list of the parameters that in addition to $M(\Lambda_c) \approx 2.28$ GeV and $m(\Lambda) = 1.12$ GeV define the semileptonic decay rate $\Gamma(\Lambda_c \to \Lambda e^+\nu)$.

After integrating the Formula 2.22 for y from 0 to y_{max}, the predicted decay rate becomes $\Gamma(\Lambda_c \to \Lambda e^+\nu) \approx 9.8 \cdot 10^{10}$ sec^{-1}. Using the experimental total decay rate[25] Γ_{Tot} for $\Lambda_c \to$ anything, the branching fraction is calculated to be $BF(\Lambda_c \to \Lambda e^+\nu) \approx (\Lambda_c \to \Lambda\mu^+\nu) \approx 1.9\%$.

2.4.2 $\Lambda_c \to PK\pi$ Hadronic Decay

The $\Lambda_c \to PK\pi$ hadronic decay is a complicated process by its nature. There are several Feynman diagrams which may represent this decay process; some of them are illustrated on Figure 2.9. The Λ_c particle either may directly decay into $PK^-\pi^+$ (See Figure 2.9(a)) or it may decay at first into one of the two quasi-particle states[26] $\Delta^{++}K^-$ (Figure 2.9(b)) or $\bar{K}^{*0}P$ (Figure 2.9(c)) and then eventually into the $PK^-\pi^+$ final state. The strong interactions are responsible for the $\Delta^{++} \to p^+\pi^+$ and $\bar{K}^{*0} \to K^-\pi^+$ decays with $BF(\Delta^{++} \to p^+\pi^+) \approx 100\%$ and $BF(\bar{K}^{*0} \to K^-\pi^+) \approx 68\%$. Theoretically it has been estimated that the W exchange mechanism (i.e., $cd \to su$; see Figure 2.9(b)) plays a significant role for the charmed baryon hadronic decay.[27] There is another complicating element in the Λ_c decay which is the interference or Pauli exclusion effect. This is because when $c \to su\bar{d}$ or $cd \to su$, then there already exists a u quark as a constituent part of the Λ_c and the newly created u quark must have restricted available spin and momentum space. The hardest part for the $\Lambda_c \to PK^-\pi^+$ decay theory is that the strong interactions (Figure 2.9(a), 2.9(b)) are involved too. In these cases $u\bar{u}$ quark pairs are created out of the color field and this process is similar to hadronization physics and, as has been discussed at the beginning of this chapter, it is not calculable. Due to these complications the latest theoretical work[28] for the Λ_c decay suggests a model. In particular, this model assumes that there is a class among the decay branches which contain a nucleon and kaon (i.e., $\Lambda_c \to NKx$ where x is a number of neutral or charged pions) and this class makes up about 50%. For the $\Lambda_c \to PK^-\pi^+ x\pi$ case, the π^+ is considered to be the mandatory particle and for the additional x pion production Poisson statistics is associated with:

$$P_x = \frac{\bar{x}\exp(-\bar{x})}{x!} \quad \text{with} \quad \bar{x} = \frac{Q}{m_\pi} \approx .7$$

where $Q = m_{\Lambda c} - (m_p + m_K + m_\pi)$ is the residual energy, $m_{\Lambda c}$=2285MeV is mass of Λ_c, and m_π=400MeV, m_p=1000MeV, m_K=600MeV are the conventional mass values for the π, p, K particles. This crude statistical model predicts $BF(\Lambda_c \to PK^-\pi^+) \approx 7\%$ and does not guarantee the accuracy better than a factor of two.

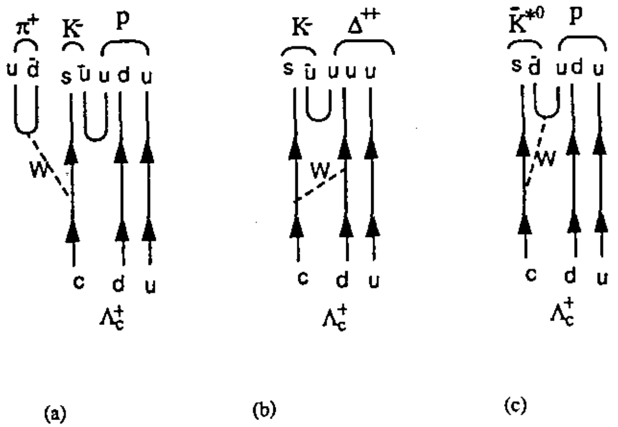

Figure 2.9 $\Lambda_c \to PK^-\pi^+$ hadronic decay. a)Λ_c decays directly into $PK^-\pi^+$ final states; b) Λ_c decays into $\Delta^{++}K^-$ with following $BF(\Delta^{++} \to p^+\pi^+) \approx 100\%$; c) Λ_c decays into $\bar{K}^{*0}P$ with the following $BF(\bar{K}^{*0} \to K^-\pi^+) \approx 68\%$ (according to LUND).

Similarly the above mentioned statistical model predicts the following hadronic decay branching fractions: $BF(\Lambda_c \to P\bar{K}^0) \approx 3\%$, $BF(\Lambda_c \to P\bar{K}^0\pi^+\pi^-) \approx 3\%$, $BF(\Lambda_c \to \Lambda\pi^+\pi^+\pi^-) \approx 4\%$.

In conclusion, there is no strict theory which could describe the hadronic decays of Λ_c's. If one resorts to experiment then the measured values[29,30] for the $\Lambda_c \to PK^-\pi^+$ branching fraction has not always been consistent and its uncertainty has not been better than 26%.

Preference

[1] F. Halzen and A.D. Martin, Quarks and Leptons, Wiley (1984).

[2] B. Andersson et al., Phys. Rep. 97, 33 (1983).

[3] T. Sjöstrand, LU TP 87-18.

[4] V.D. Barger, R. Phillips, Collider Physics (1987).

[5] V.D. Barger, R. Phillips, Collider Physics (1987).

[6] J. Schwinger, Phys. Rev. 82, 664 (1951).

[7] A. Casher et al., Phys. Rev. D20, 179 (1979).

[8] B. Andersson et al., Z. Physik C6, 235 (1980).

[9] B. Andersson et al., Phys. Rep. 97, 33 (1983).

[10] The best tuned LUND5.3 parameter values at E_{cm}=29 Gev are estimated by T.Edberg, Berkeley.

[11] C.D. Buchanan and S.B. Chun, Phys Rev. Lett. 59, 1997 (1987) .

[12] C.D. Buchanan and S.B. Chun, UCLA-HEP-90-003 (1990).

[13] Sebong Chun, PhD Thesis, University of California, Los Angeles (1989).

[14] C.D. Buchanan and S.B. Chun, preparing for the publication.

[15] B. Andersson and G. Gustafson, private communiciation.

[16] K.G. Wilson, Phys. Rev. D10, 2445 (1974).

[17] B.R. Webber, Nucl. Phys. B238 , 492 (1984).

[18] D. Gottschalk, Nucl. Phys. B239, 349 (1984).

[19] G. Marchesini, Nucl. Phys. B238, 1 (1984).

[20] M. Bengtsson et al., LU TP 86-24.

[21] Sebong Chun, PhD Thesis, University of California, Los Angeles (1989).

[22] R. Perez-Marcial et al., Phys. Rev. 40D, 2955 (1989).

[23] Robert Singleton Jr., SLAC-PUB-5335, (1990).

[24] Robert Singleton Jr., SLAC-PUB-5335, (1990).

[25] Review of Particle Properties, Phys Lett. B239, (1990).

[26] J. G. Korner et al., Phys. Lett. B78, 492 (1978).

[27] B. Guberina et al., Z. Phys. C-Particles and Fields 33, 297 (1986).

[28] J. D. Bjorken, Unpublished Draft dated July 7 (1986).

[29] G.S. Abrams et al., Phys. Rev. Lett. 44, 10 (1980).

[30] P.Avery et al., CLNS 90/992, CLEO 90-5, June 1990.

Chapter 3. Experimental Apparatus

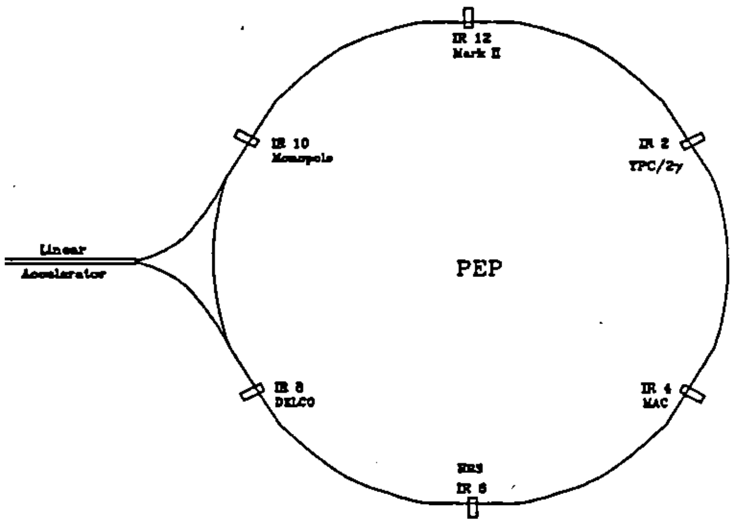

Figure 3.1 Schematic view of Positron Electron Project ring. The locations of the six Interaction Regions are shown.

This experiment was performed at one of the interaction regions of the Positron Electron Project (PEP) storage ring where the TPC/2γ detector facility is installed (see Figure 3.1, 3.2). The two mile Linear Accelerator (LINAC) accelerates electrons and

positrons up to 14.5 GeV energy level and then injects them into the PEP storage ring.[1] The purpose of the PEP storage ring is to compensate the circulating electrons' and positrons' energy losses due to synchrotron radiation and then bring these electron and positron matter and antimatter particles into head on collisions. The klystrons are placed along the LINAC in order to supply the boosting energy. Along the PEP storage ring, the dipole magnets are installed in order to circulate the beams and a series of quadrupole and sextupole magnets are installed, with alternating magnetic poles, in order to focus the beams. A series of RF cavities around the PEP ring compensates the electrons' and positrons' synchrotron radiation energy losses. The electron-positron beam-beam interaction region is surrounded by the TPC/2γ detector complex which is designed to register relatively stable elementary particles. The registered data is analyzed by the physicists of the PEP 4/9 collaboration. In this experiment in which we were dealing with the tiniest elementary particles known in the universe, the time measurement accuracy sometimes was often order of hundreds of picoseconds, the spatial measurement resolution was of the order of a few hundred micrometers, the dimensions of whole apparatus was up to a couple of miles, the weight of TPC/2γ detector by itself was of the order of thousands tons, the number of scientists and technicians who have worked on this project over the decades was in the hundreds. All these, unmistakably, may qualify the SLAC facility as one of the technological wonders in this world.

In this dissertation only the essential and relevant components of the experimental apparatus are discussed. In the following sections, the various components of the detector are discussed according to their radially increasing physical locations (see Figure 3.3). The representation of the apparatus setup applies only for the configuration of December 1984 up to March 1986.

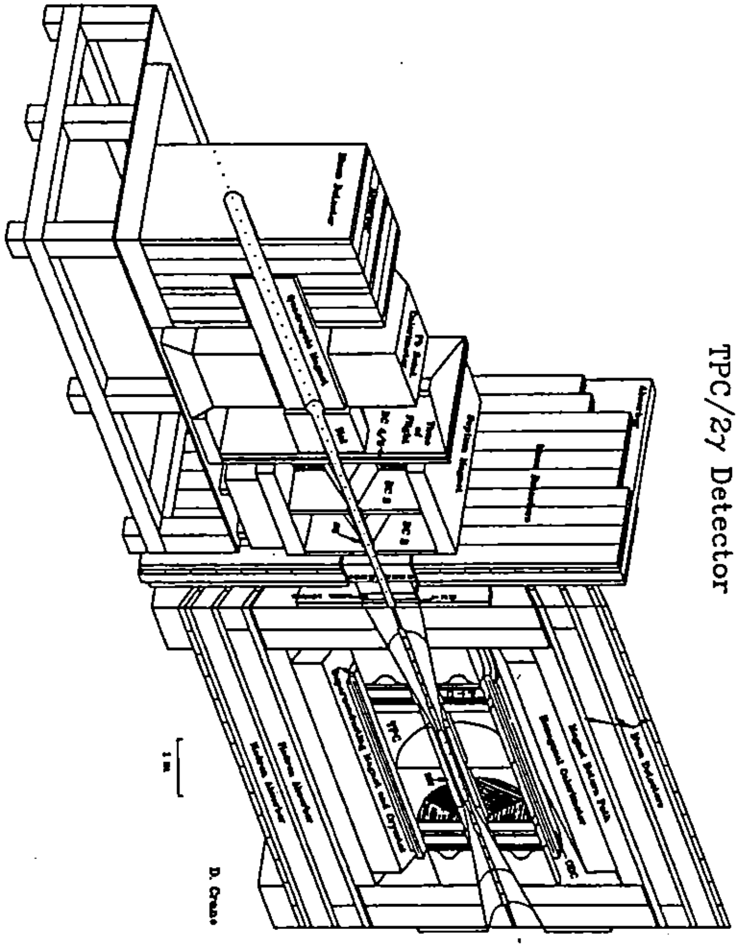

Figure 3.2 TPC/2γ detector facility during the 1985-86 data taking. Only one arm of the forward detectors is displayed.

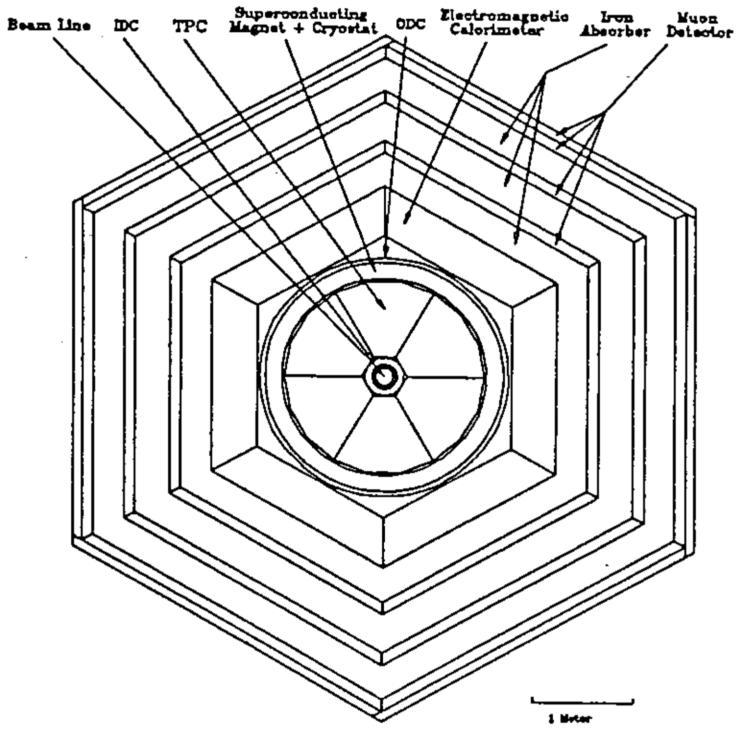

Figure 3.3 The transverse cross section of TPC/2γ detector.

3.1 Beam Pipe

One of the essential parts of the PEP storage ring is the beam pipe through which the electrons and positrons navigate in opposite directions. The overall circumference of the beam pipe is about 2.2 km and the beam pipe becomes straight around the interaction region. The length of the straight pipe is about 100 meters. The straightness of the beam pipe at the interaction region protects the detector's sensitive volume from synchrotron radiation contamination. The radiation loss per second of the circularly moving relativistic particle has energy (E) and curvature (ρ) dependence: $P \propto \frac{E^4}{\rho^2 m_e^4}$. The beam pipe is made of aluminum in a cylindrical form with 8.5 cm inner radius. The pipe thickness is about .2 cm. To avoid beam gas interactions, high vacuum (10^{-8} Torr) is created inside the beam pipe. During data taking, the electrons or positrons were grouped into three bunches of each. The size of each bunch was typically 500μm×50μm×1.5cm and the distribution of the electrons and positrons within the bunch were Gaussian in any coordinate direction. The typical Luminosity for this experiment was 1.2×10^{31} cm^2/sec.

3.2 Inner Drift Chamber

The Inner Drift Chamber[2] (IDC) is located outside of the beam pipe and it embraces the inner pressure wall. The IDC occupies 13.2-19.4 cm in radial dimensions and is 114.3 cm long. The IDC has 240 sense wires and 480 field wires, which are parallel to beam axes. The sense wires are distributed within four layers where each layer contains 60 sense wires. Between layers, the azimuthal angle difference between the neighbor sense wires is

6°. The second and fourth layers are shifted by 3° relative to first and third layers. The IDC uses TPC exhaust gas, a mixture of 80% argon and 20% methane gases which was fixed at 8.5 Atm pressure.

3.3 Time Projection Chamber

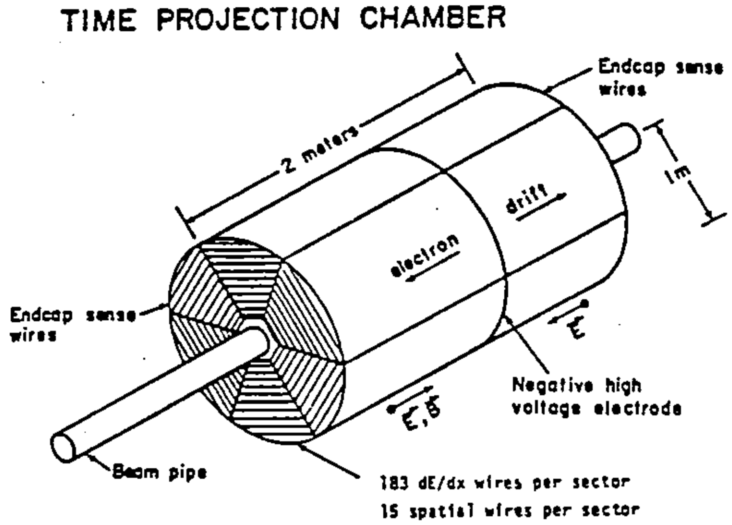

Figure 3.4 Time Projection Chamber layout. The six endcap sectors, the membrane, and the direction of the uniform electric and magnetic fields are shown.

The Time Projection Chamber[3] (TPC, see Figure 3.4) is the central element in our detector complex and it is not accidental that the whole detector system is named "TPC/2γ detector". Thanks to the TPC, the charged particles' mass (i.e., particle identification), 3-dimensional trajectory, and momentum were determined. Due to its significance, the TPC is discussed in more detail. The physical features of TPC are the followings: it has a cylindrical shape with inner and outer radius .20 m and 1 m, respectively. The TPC length is about 2 m and it is terminated at both ends with endcaps. The TPC is filled with a gas mixture of 80% argon and 20% methane. The gas environment is maintained at 8.5 Atm constant pressure and at T=298 ^{0}K constant temperature. Below the configuration of the electric and magnetic fields, and the electronics setup is described. A thin membrane which has annular form bisects the TPC into two equal pieces. The membrane was set at -50 kv equipotential level for the first half of data and at -55 kv level for the second half of data. Both endcaps were held at ground level potential. The inner and outer field cages, endcaps, and the membrane shape the uniform electric field which is directed from the endcap to the membrane. Inside the TPC volume, the uniform magnetic field is created by the superconducting coil located outside TPC. The dimensions of the coil are 2.25 m in diameter and 3.12 m in length. The magnitude of the magnetic field is 13.5 kgauss and is oriented parallel to the electric field lines and beam axes.

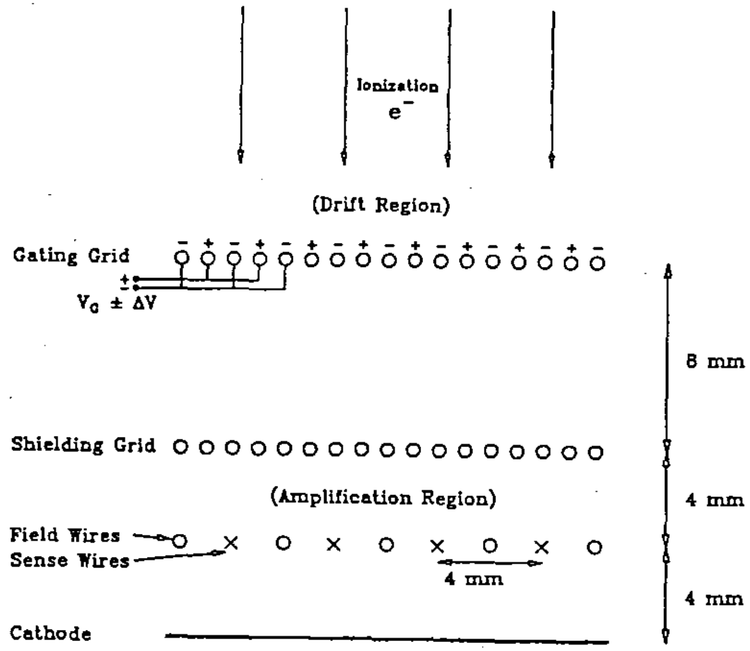

VOLTAGES

Midplane	−55 kV	
Gating Grid	−910 V ± 90 V	(Opaque Mode)
	± 0 V	(Transparent Mode)
Shielding Grid	0 V	
Field Wires	700 V	
Sense Wires	3400 V .	
Cathode	0 V	

Figure 3.5 The wiring configuration in each TPC sector.

The proportional wire system at the inner endcap surface reads out the signals. There are three wire layers just above the endcap inner surface and one pad layer just on the endcap surface. All this wire system has six fold symmetry, thus it is sufficient to discuss only one sector (or part) of this wire system. The uniformity of the electric field inside TPC detector breaks around the first wire layer which is called the Gating Grid (see Figure 3.5). The Gating Grid represents a series of parallel wires which are installed 16 mm away from the endcap and inside the TPC. The Gating Grid wires are 1 mm apart from each other. The consecutive wires have alternating voltage v=910+/-90v and under special circumstances all wires may have V=910 v equal potential. The next wire set is the Shielding Grid wire set which is 8 mm from endcap and Gating Grid wire set. The Shielding Grid wires are 1 mm apart from each other and are running parallel to the Gating Grid wire set. The Shielding Grid wire set is held at ground level voltage at all times. There is another wire layer which is located between the Shielding Grid wire set and the endcap surface. This wire set is 4 mm from the Shielding Grid wire set and endcap surface. This wire layer represents alternating Sense and Field wires which are separated by 2 mm from each other. The Sense wires are held at 3400v constant potential level, and the Field wires are held at 700 v potential level. There are overall 185 Sense wires and 184 Field wires (see Figure 3.6). Finally, there are 15 pad rows on each sector's inner surface. Each Pad row is just beneath the following 13-th Sense wire. The pads electrically are isolated from one another and each pad has 7.5mm×7mm active surface. Each pad is held at ground level potential. The TPC overall has 13824 cathode pads and 2196 active Sense wires and each pad or Sense wire has one separate electronics channel (see Figure 3.7).

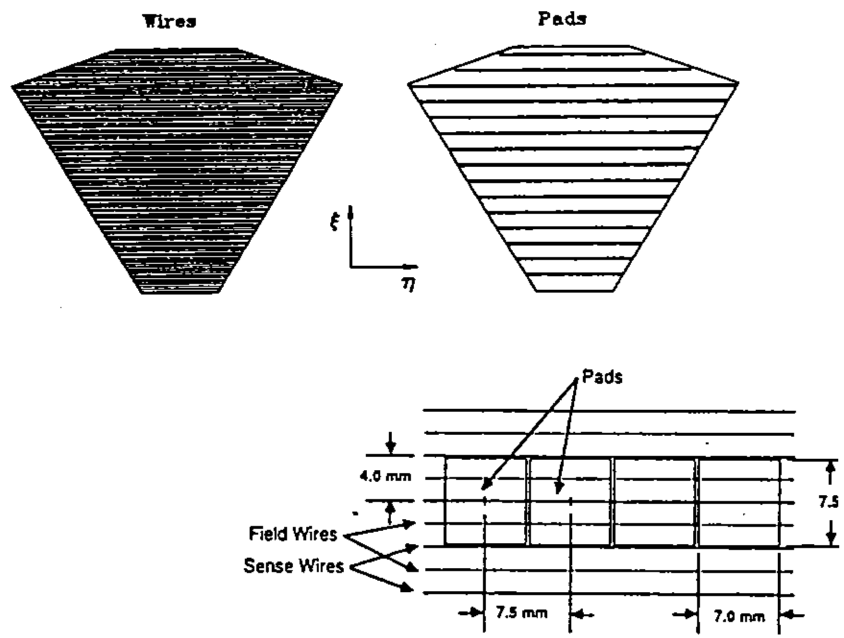

Figure 3.6 The TPC sector layout. 185 sense wires and 15 pad rows are displayed. The magnified view of the pad row segment is shown too.

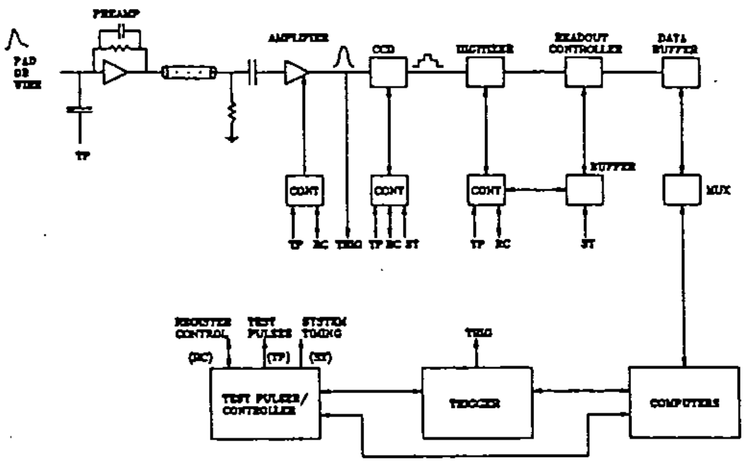

Figure 3.7 The schematic diagram exhibiting the signal processing patterns for a single pad or Sense wire electronics channel.

There are several reasons which make argon (Ar) an attractive candidate as a "base" working gas inside the TPC. First of all, it is an inert (noble) gas. Second, argon atoms basically do not have absorption energy levels lower than the primary ionization energy level because of the absence of the vibrational freedom of movement. This makes it easier for the accelerating electrons to reach the ionization energy level and to produce the secondary ionization. This property of argon gas allows lower operational voltage for the same gain. The third reason is that the ionization energy loss per cm is proportional to the density (the weight per unit volume) of the gas medium. Xe and Kr, heaviest noble gases,

are good candidates and satisfy all these conditions, but argon gas is considerably less expensive. Within the TPC environment there are two sources which generate photons. These photons are capable of reaching the cathode and liberating electrons which eventually can generate an undesirable self-sustaining electrical discharge. One of these photon sources is a result of electron capture by the positive argon ions around the avalanche region. The second photon source originates when the argon ions neutralize at the cathode. By mixing methane "quench" gas (CH_4) with the argon gas (1:4 proportion), this problem is solved. The characteristic of the methane polyatomic gas is that it has many vibrational and rotational energy levels and easily absorbs photons. The excited methane gas atoms either transfer their excess energy to their colliding partners through inelastic collisions and fall into the ground level or break up into pieces (decompose). Then, since methane atoms have lower primary ionization energy (13.1 eV for methane atom versa 15.8 eV for argon atom), it is highly probable that an electron would be transferred from the methane atom to the positive argon ion when they collide with each other. The methane ion after reaching the cathode decomposes, in contrast with the argon ion case where the photon was emitted. Therefore, the above mentioned undesirable photon sources are eliminated due to methane gas presence.

As a charged particle from the e^+e^- interaction travels through the TPC gas medium, it ionizes the surrounding gas atoms. For any massive relativistic elementary particle (e.g., μ, π, K, P) the main source of energy loss is due to ionization. According to classical calculations, the energy transferred to the atomic electrons is about 4000 times more than the energy transferred to the nucleus. This is because the assumption of equal momentum transfer (due to equal Coulomb force and interaction time) into nuclei and electrons leads to the conclusion that the transferred energy should be inversely proportional to the mass of the target particles. The liberated electrons drift towards the endcaps and the positive ions towards the central membrane. The axially directed magnetic field substantially prevents the drifting particles from diffusing into the transverse directions. The drifting electrons first approach the Gating Grid. Under normal conditions the drifting electrons are absorbed by the Gating Grid due to the V=-910+/-90 v voltages on the alternating wires of the Gating Grid. It is worth mentioning that the main purpose of the Gating Grid installation is the neutralization of the positive ions which otherwise may enter into the TPC drift region and build a space charge. The space charge may distort the homogeneity of the electric field and the drifting electrons may carry misleading information about the initial ionization location. Under special conditions (when the Trigger is set) the Gating Grid acquires V=-910 v equipotential level. The Gating Grid voltage is chosen carefully so that the electric field lines running between the sense wires and the central membrane would not terminate on the Gating Grid wire set. In this case the Gating Grid permits the drifting electrons to pass through the "gate".

After passing the Gating Grid, the drifting electrons approach the "Shielding Grid". The Shielding Grid is set at ground potential level and it has the purpose to "Shield" the drifting region from the avalanche region. The avalanche region is around the sense wire and it extends to a size of a few radii in the radial direction. The voltage on the Field wire is chosen such that it prevents the avalanche signal crosstalk between the Sense wires.

The electric field lines become very dense around the Sense Wire vicinity where the avalanche occurs. The potential level on the Sense wires is chosen such that the collected charge on the Sense Wire is proportional to the number of electrons in the initial ionization. Each Sense wire is electrically connected to a Charge Sensitive Preamplifier which generates voltage output proportional to its input charge. The Shaper Amplifiers are used in

order to amplify the Preamplifiers output voltage. The output of the Shaper Amplifier is sampled every 100 ns within a 45 μs time span,[4] which covers the maximum drift time required for the electrons to drift from the central membrane to the sense wires. The device responsible for this function is a Charge Coupled Device (CCD). These sampled signals ("buckets") are digitized and afterwards are compared with the previously stored threshold values ("Lower-Limit RAM's"). The "buckets" which are above the Lower-Limit RAM values are permitted to propagate from the digitizer into a memory buffer. The number of "buckets" which are above Lower-Limit RAM (LLR) values typically are 5 to 7 per channel and per track. The bucket number represents the sampling time which can be converted into the z (axial) coordinate of the track by multiplying it with drift velocity. The drift velocities are 3.33cm/μs, 3.25cm/μs when the membrane voltages were held -50kv and -55kv, respectively.

To reconstruct 3-dimensional track for the charged particle, at first 15 space points are determined then track fitting algorithm is applied. 15 space points are determined by using 15 pad rows and related Sense Wire information. The η position (see Figure 3.6) of the track is determined by fitting a Gaussian to the disturbed pad channels. Since the signal on the pad channel can be induced from the nearest 5 sense wires then the ζ position of the track is determined by estimating amplitude-weighted-average ζ position of corresponding 5 wires. The z position of the track is determined by estimating amplitude-weighted-average z position of corresponding 5 wires. The η, ζ, and z measurements' uncertainties are 150μm,150μm, and 200μm, respectively. The "pattern recognition" algorithm applies a "histogram" technique to reconstruct the projectiles' 3-dimensional track. The "histogram" algorithm determines the tracks with 97+/-2% efficiency when there are at least three pad hits. After determining the tracks in 3-dimensional space, the momenta can be measured for the given magnetic field. For the well reconstructed tracks the momentum uncertainty is:

$$\frac{\delta P}{P} = \sqrt{(.015)^2 + (.007\ P\ Gev^{-1})^2}$$

where the first term under the root sign is due to uncertainty caused by the Coulomb scattering and the second term is due to uncertainty of the track finding and fitting.

Besides finding the particles' track and trajectory, the TPC has another important function which is to provide the particle identification (ID). The TPC uses the incoming particle's ionization energy loss rate information in order to find the particle ID. In this experiment the velocity of the projectile particle is larger than the velocity of the orbiting electrons inside the atom ($\sim\alpha c$), and the projectile velocity is small enough that Čherenkov radiation can be ignored. In this case, the average ionization energy loss rate of the unit charged non electron projectile which passes through a homogeneous medium is given by the Bethe-Bloch equation:[5]

$$-\frac{dE}{dx} = \frac{0.154}{\beta^2}\frac{Z}{A}\left[\mathrm{Log}\left(\frac{2m_e}{I}\right)^2 + 4\mathrm{Log}\gamma\beta - 2\beta^2 - \delta\right]$$

where E is incident particle energy in units MeV;

x is incident particle traveling distance inside gas medium in units g/cm^2;

A is the atomic weight in grams per mole;

Z is the nuclei atomic number for the gas medium;

β is the incident particle velocity and $\gamma = \frac{1}{\sqrt{1-\beta^2}}$;

$I = (9.76Z + 58.8Z^{-.19})$eV is the average ionization potential where all orbital atomic electrons are involved in the averaging process;

δ is the medium density effect.

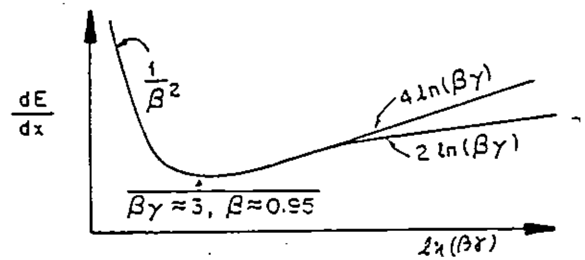

Figure 3.8 The theoretical prediction for dE/dx ionization energy loss rate vs Log$\beta\gamma$. The lower curve is obtained after taking the density effect into account. (Reproduced from the reference 6, Chapter 3)

The accuracy of the Bethe-Bloch formula is within a few percent for any incident particle velocity. The characteristics of the dE/dx curve are the following (see Figure 3.8): for an incident particle with velocity larger than αc (where $\alpha = 1/137$) but less than $\gamma \approx 3.2$, dE/dx falls like $\sim 1/\beta^2$. It reaches a minimum value around $\gamma \approx 3.2$. As β increases further (relativistic rise region), the dE/dx slowly increases due to the relativistic expansion of the transverse electric field of the incoming charged particle. In reality, the dE/dx increases as a function of 2Logγ (instead of 4Logγ) due to the density effect. The density effect is a polarization phenomenon (charge screening) generated by the orbiting atomic electrons of the medium. For argon gas medium, the density effect can be parametrized[6] according to:

if $2.02 < \mathrm{Log}_{10}(\beta\gamma) < 5$ then $\delta = 4.606y + C + .0255\,(5-y)^{4.36}$

if $\mathrm{Log}_{10}(\beta\gamma) > 5$ then $\delta = 4.606y + C$

where $y = \mathrm{Log}_{10}(\beta\gamma)$ and $C = \mathrm{Log}(I_{plasma})^2 - \mathrm{Log}(I_{Ioniz.Pot})^2 = -12.27$. Observation shows that for large $\beta\gamma$ values, when $\mathrm{Log}_{10}(\beta\gamma) > 5$, then δ becomes equal to $\delta = 4.606\mathrm{Log}_{10}(\beta\gamma) + C = 2\mathrm{Log}(\beta\gamma) + C$. Therefore, in this region, where $\mathrm{Log}_{10}(\beta\gamma) > 5$, dE/dx increases as $2\mathrm{Log}(\beta\gamma)$. Then, the dE/dx behavior in the relativistic rise region with upper boundary

$Log_{10}(\beta\gamma) < 5$ is $2Log(\beta\gamma) + .0255\,(5\text{-}y)^{4.36}$. For the TPC mixed gas environment, the ionization energy loss rate[7] is $\frac{dE}{dx} = \sum_{i=1}^{2} f_i \frac{dE}{dx_i}$, where f_1, f_2 are the weight fractions of the argon and methane gas components.

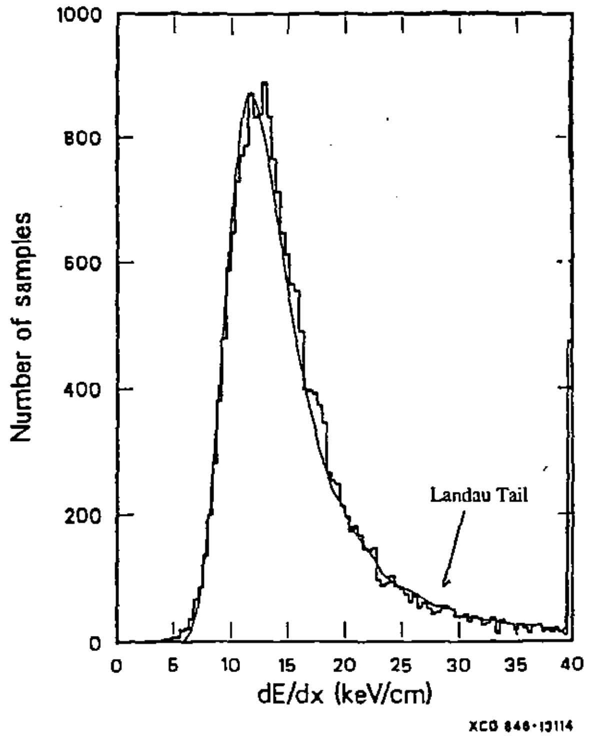

Figure 3.9 dE/dx samples' distribution for minimum ionizing pions with 4 mm track segments.

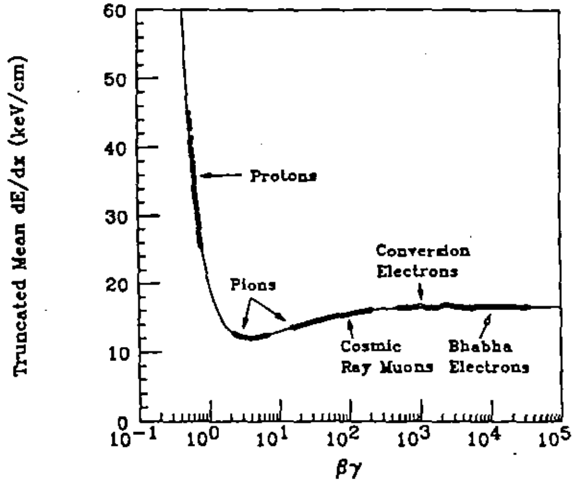

Figure 3.10 dE/dx vs Logβγ fitting curve is obtained by using variety particle samples for different βγ range.

So far the energy loss rate for the incoming particle has been discussed in a format which turns out to be practically different from the measured (detected) ionization energy loss rate. The statistics of the dE/dx ionization energy loss within a restricted track segment (e.g., 4 mm, see Figure 3.9) is characterized by a Gaussian distribution when large amount of electrons carry relatively small energy after the collision. The projectile and atomic electrons collision also creates rare knock-on electrons which add Landau-tail signature to the Gaussian distribution. The Landau tail behaves like $\frac{1}{\varepsilon^2}$, where ε is knock-on electron (δ-ray) energy. This allows an infrequent, but very large energy deposition. A truncated mean technique is applied in order to avoid this infrequent but large contribution into average ionization energy loss measurement. In the truncated mean technique only the lowest 65% of the dE/dx samples from TPC Sense wire signals are used in order to extract the mean dE/dx value. In this case, the truncated dE/dx value is very close to the peak value (the most probable value) of dE/dx distribution. The usage of this technique reshapes the dE/dx curve further where the relativistic rise eventually saturates (the "Fermi Plateau" region). Since there is no theory or model which describes reality perfectly, a fitting curve is used as a reference. By using the following particles: protons, pions, Cosmic Ray muons, conversion electrons, and electrons-positron outgoing particles from Bhabha events in variety velocity ranges, the dE/dx vs Log$\beta\gamma$ fitting curve has been constructed (See Figure 3.10). The estimated systematic uncertainty of the fitting curve is about 0.2%. A spectrum of dE/dx fitting curves could be created if the Log$\beta\gamma$ variable is substituted by LogP, where P is the particle momentum, p=m$\beta\gamma$. The offset between two fitting curves in abscissa coordinate for m_1 and m_2 incident particles must be equal to $|\mathrm{Log}m_1\text{-}\mathrm{Log}m_2|$. Therefore, the fitting curves readily are obtained for the directly observable particle: e, μ, π, K, and P (See Figure 3.11).

In order to identify the particle, the dE/dx truncated mean ionization loss value is measured simultaneously with the momentum P. Then the χ_i^2 values are determined according to:[8]

$$\chi_i^2 = \mathrm{Min}\left[\frac{(P-P_i)^2}{\delta P^2}\frac{P_i}{P} + \frac{dE/dx - (dE/dx)_i^{\,2}}{\delta(dE/dX)^2}\right]$$

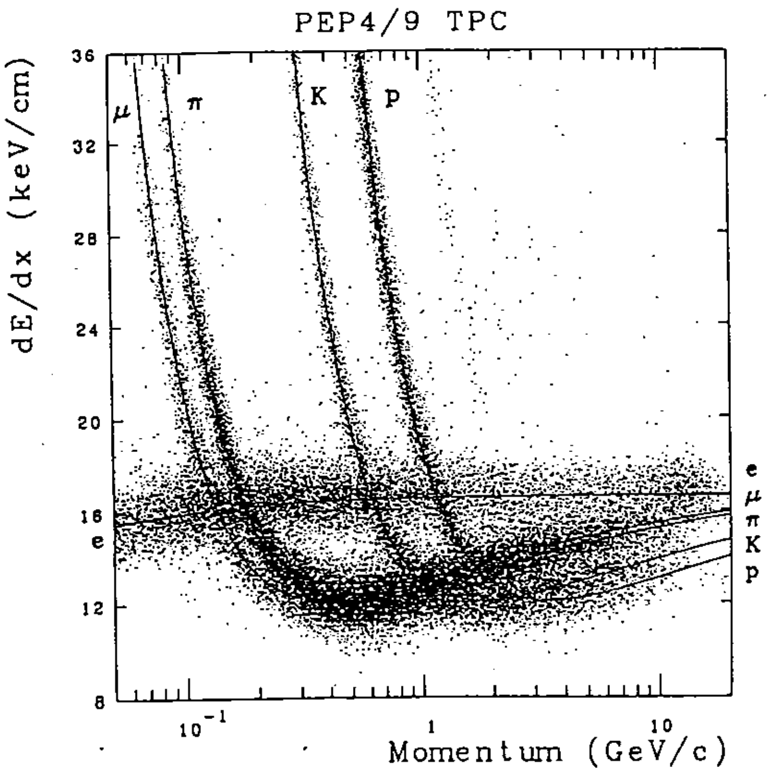

Figure 3.11 (dE/dx,P) scatter plots for e,μ,π,K,P particles where dE/dx is measured truncated mean value. The fitting curves also are displayed.

where the (P_i, dE/dx_i) pair denotes the coordinates of the dE/dx vs P fitting curve, when i = e, μ, π, K, and P. In this dissertation, the "hadron probability" (hadprob) concept is used in order to identify the long living particles. This is because the particle identification at "Fermi Plateau" region, or around the crossover regions in the dE/dx vs P curves is not unique. To alleviate this problem, the particle fractions as a function of momentum are used, where the particle fractions are determined based on the "good hadronic events" (discussed later). Since the hadronic events containing at least one muon are rare, the hadron probability algorithm is applied only for the e, π, K, and P particles. The particle hadprob is determined:

$$W_i = N\, f_i(P)\, \exp(-\tfrac{1}{2}\chi_i^2)$$

where N is the normalization constant so that $\sum_{i=1}^{4} W_i = 1$.

3.4 Outer Drift Chamber

The Outer Drift Chamber[9] (ODC) is composed of three coaxial cylindrical layers. The three layers conventionally are labeled E, F, and G and have radii 119.7 cm, 121.7 cm, and 123.8 cm, respectively. The drift chamber is 310 cm long and centered at the interaction point. Each layer is divided into 216 cells and at the center of each cell a single sense wire is stretched. The ODC neighbor layers are azimuthally shifted from each other so that the ODC chamber accomplishes better azimuthal angle measurement accuracy. The ODC chamber uses TPC exhaust gas, 80% argon and 20% methane, at one atmosphere

pressure. The main purpose of the ODC is to supply fast trigger signals. The ODC also has a second application, to aid in the photon energy estimated by the HEX calorimeter (discussed in section 3.5). There are some fraction of photons which develop early showers in the magnetic coil. Since ODC is located between the magnetic coil and HEX calorimeter, the ODC information can be used to correct the early photon-induced shower energy.

3.5 Hexagonal Calorimeter

The purpose of the Hexagonal Calorimeter[10] (HEX) is to measure electron, positron, and photon energies. The HEX covers 75% of 4π and it is composed of 6 identical modules. Each module has 3.84 m length and trapezoidal transverse cross-section. The depth of every single module is 36 cm and each module represents a sandwich of 40 lead-laminates/drift-chamber layers. The overall thickness of lead layers in units of radiation length is 10.4. Both laminate surfaces are divided into parallel strips. The width of a single strip, as seen from the interaction point, is 8 mrad or 10 mrad depending on whether the strip is located in the front (27 layers), or rear (13 layers) HEX section. One laminate surface has strips with orientation +60° with respect to the beam axes, the other one -60°. Halfway between the laminates, the sense wires run parallel to the beam axes. The separation between the sense wires is 5 mm. The HEX is filled with a mixture of 92.3% argon, 5.5% methylal, and 2.2% nitrous oxide at one atmosphere. The HEX operates in Geiger discharge mode. There are also nylon filaments running perpendicular to sense wires with 10 mm separation. These filaments restrict the avalanche processes within 10 mm in length along the sense wire. During the avalanche, the signals are induced on the surface strips above and below the sense wire. These induced signals, in conjunction with the sense wire signals, provide three-stereo views of Geiger discharge. The total number of Geiger discharge is proportional to the incident initial particle energy. The proportionality constant is about 6 MeV per Geiger discharge. The HEX energy measurement resolution is $\frac{\delta E}{E} = \frac{17\%}{E^{1/4}}$, where E is in GeV. The main contribution to the energy measurement uncertainty is due to the uncertainty of energy escape and the uncertainty of energy absorption by the magnetic coil.

3.6 Muon System

The Muon system[10] covers 98% of 4π. In the central region, the Muon system has a hexagonal shape and consists of four layers of triangular drift tubes. There is a single sense wire at the center of each tube. The drift tube units of the first three layers are parallel to beam axes. The drift tube units of fourth layer are perpendicular to the beam axes. The iron slabs, which overall have 90 cm thickness, are sandwiched between the layers. The Muon detector uses TPC exhaust gas: 80% argon, 20% methane at 1 atmosphere. The Muon detector operates in the proportional mode. The muon detection efficiency is 99%.

3.7 Pole-Tip Calorimeter

The Pole-Tip Calorimeter[12] (PTC) has a cylindrical shape and is a sandwich of 51 layers of lead-laminates and Multiwire Proportional Chambers. Overall lead-laminates' thickness in units of radiation length is about 13.5. The Pole_Tip Calorimeter modules are installed on the iron pole tips which returns the magnetic flux. Overall two PTC modules cover 18% of 4π. The sense wires are placed halfway between the laminates, and the wires in each layer are rotated by 60° with respect to wires in the neighbor layers. This gives a 3-stereo view for a single hit. The PTC is inside TPC gas volume and operates in proportional mode. The PTC measures the incoming electron, positron, and photon energy by using electromagnetic shower evaluation algorithm. The total sum of the signals from all channels is proportional to the incident particle energy. The PTC is both monitors the luminosity and also provides electron, positron, and photon information for particles from the e^+e^- interaction.

3.8 Forward Detectors

There are several detectors as a part of Forward detector system[13] which are used to observe or reject low angle electrons as a resulting from photon-photon interaction. The Forward Detectors consist of 5 Drift Chambers, one Čherenkov counter, a Time-of-Flight scintillator hodoscope, a NaI Calorimeter, a lead-scintillator Shower Counter, and a Septum Magnet. In the following data analysis sections, no important information has been used from the Forward Detector, and we do not discuss it here in detail.

3.9 Trigger

Special conditions[14] ("Triggers") must be satisfied in order to collect the potentially interesting events. The multihadronic events are required to pass three trigger levels.[15]

3.9.1 Pre-Pre-Triggers

The pre-pre-trigger makes a decision while the Gated-Grid still is in opaque condition. The pre-pre-trigger uses IDC, ODC and prompt TPC information. In this case prompt TPC signals is generated when the incoming charged particle crosses the endcap. For triggering purposes, the TPC endcap is segmented into supersectors (see Figure 3.12). The supersector is made of two adjacent sectors where the sense wires with similar radial location are logically "ORed". The pre-pre-trigger is set either (a) if within a 0.5 μs time window after the beam-crossover there are coincidence hits on both the ODC and IDC sectors covering the same azimuthal angle range ($\Delta\phi=30^{\circ}$), or (b) if there is a prompt signal on the TPC supersector within a 1.7 μs time window after the beam-crossover in conjunction with a hit in the second or third IDC sectors counted from the edge of the active supersector. After satisfaction of the pre-pre-trigger condition, the Gated Grid is switched to "transparent".

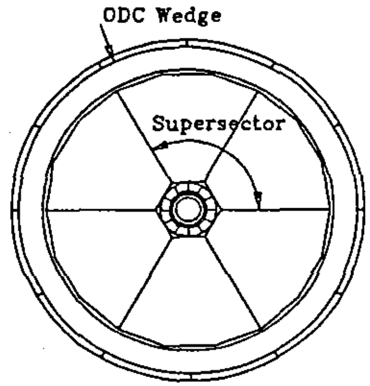

Figure 3.12 TPC supersector configuration is shown. 12 ODC and IDC dodecants can be observed.

3.9.2 Pre-Triggers

For triggering purposes, 183 sense wires from the TPC supersector are ganged into 23 "majority units", where each unit contains 8 consecutive wires. Here, the lower wire group number corresponds to smaller radial location. Majority hit (or majority signal) is defined for the individual group, if there are at least 4 hits in that particular wire group. The following conditions are used for a pre-trigger decision:

Condition_A: There is a coincidence hit on both IDC and ODC sectors within the same azimuthal angle range, $\Delta\phi=30^{\circ}$.

Condition_B: There is a majority hit with minimum group number equal to 6, which occurs within a 3 μs time window after 3.3 μs of the beam-crossover.

The pre-trigger is set if (a) two charged particles satisfy Condition_A, (b) one charged particle satisfies Condition_A and another particle satisfies Condition_B, (c) two charged particles satisfy Condition_B under the precondition that two involved supersectors are non-adjacent.

3.9.3 Final Triggers

A "ripple" is generated if there are a sequential majority hits with decreasing group number and increasing arrival time which terminates at a majority unit number 0 or 1 within a proper "Ripple time" window. The "ripple" is not considered complete if there are three consecutive wire groups without a majority hit. The trigger is set if there are two tracks which generate two complete "ripples".

The trigger can be generated alternatively if another set of conditions are satisfied. There are three "Radial Majority Latches" designed for each endcap. The "Radial Majority Latch" is an output of six logically "ORed" inputs where each input is a majority signal out of eight consecutive majority units. Here, the majority signal is present if at least four majority units out of eight have hits. Again, each majority unit is composed of eight consecutive wires which belong to the same sector. The majority unit is considered to have a hit if at least four out of eight consecutive wires have hits. Each "Radial Majority Latch" covers all sectors within certain radial range (64 wires). The majority trigger is set if there

is one complete ripple and all three "Radial Majority Latches" are set within Majority time window. The Majority time window is designed such that within that time interval the ionization which occurs around the central membrane is expected to arrive at the endcap. Thus the majority trigger is designed for two charged particles when one of them makes about 90° relative to beam axes.

References

1 R.B. Neal, The Stanford Two-Mile Linear Accelerator, W.A. Benjamin (1968).
2 W. Gorn et al., IEEE Trans. Nucl. Sci .26, 68 (1979).
3 H. Aihara et al., IEEE Trans. Nucl. Sci. 30, 63 (1983).
4 H. Aihara et al., IEEE Trans. Nucl. Sci. 30, 76 (1983).
5 U. Fano, Ann. Rev. Nucl. Sci. 13, 1 (1963).
6 K. Ticho, Elementary Particle Laboratory Lecture Notes, UCLA (1985).
7 Review of Particle Properties, Physics Letters, 239B (1990).
8 A. Barker, "On the Formation by Photon-Photon Fusion of Resonances Decaying to $\pi^+\pi^-\pi^0$ and $\eta\pi^+\pi^-$", PhD Thesis, University of California at Santa Barbara (1988).
9 H. Aihara et al., IEEE Trans. Nucl. Sci. 30, 153 (1983).
10 H. Aihara et al., IEEE Trans. Nucl. Sci. 30, 117 (1983).
11 H. Aihara et al., IEEE Trans. Nucl. Sci. 30, 67 (1983).
12 C. Buchanan et al., In Proceeding Of The Gas Calorimeter Workshop, p.284, Batavia, IL (1982).
13 M.P. Cain et al., Phys. Lett. 147B, 232 (1984).
14 A. Barker, "On the Formation by Photon-Photon Fusion of Resonances Decaying to $\pi^+\pi^-\pi^0$ and $\eta\pi^+\pi^-$", PhD Thesis, University of California at Santa Barbara (1988).
15 M. Ronan, J. Millard and T. Mcgathen, IEEE Trans. Nucl. Sci. 29, 427 (1982).

Chapter 4. Measurement of Λ_c Production

4.1 Event Selection

The carefully selected "Good Multihadronic" events are used in the following data analyses. The selection of these events is based on the "good" tracks. A track is considered to be a "good" track if it satisfies the following conditions:

1) The distance between the closest approach of the extrapolated track and the nominal primary vertex point in the xy plane and in the z coordinate satisfies xy< 6 cm, z< 10 cm, respectively.

2) The polar angle between the track and the beam axes is more than 30°.

3) The track momentum is larger than 120 MeV/c.

4) The uncertainty of the measured curvature ($C=\frac{1}{\sqrt{P_x^2+P_y^2}}$) is less than .3 $(\mathrm{GeV/c})^{-1}$ or the curvature resolution is less than 30% (i.e., $\frac{\Delta C}{C} < .3$).

An event which already has satisfied the trigger condition is considered to be a "Good Multihadronic" event if:

1) The event contains more than 5 "good" non-electron tracks in it. The electron is identified by using the dE/dx information or by using the Pair Finder algorithm. The Pair Finder searches and identifies e^+e^- pairs which most probably are the result of pair production processes from photons interacting in material.

2) More than 50% of the observed tracks are "good" tracks.

3) The energy sum of all charged tracks is at least 7.25 GeV.

4) The absolute sum of the momentum projections on the beam axes satisfies $\Sigma|P_z|<.4E_{cb}/c$.

5) There is at least one hemisphere where the invariant mass of the charged tracks is more than 2 GeV/c^2 or there are more than 3 charged tracks.

6) The location of the reconstructed event vertex is within a geometrical cylinder of radius 20 mm and length 70 mm which is oriented parallel to the beam axes and centered at the nominal interaction point.

The data collected during December 1984 to March 1986 has 68pb^{-1} total integrated luminosity and contains 25782 "Good Multihadronic" data events. The purity of genuine hadronic events within the "Good Multihadronic" sample is about 98%. In the following data analyses only "Good Multihadronic" events, defined as above, are used. Within these events the tracks, hadronic or non-hadronic, were subject to "tight" cuts: the Z coordinate is required to satisfy z< 5 cm; the polar angle between the track and the beam must be larger than 35^o; the track momentum must be larger 150 MeV/c and the track curvature uncertainty must be less than 0.15 (GeV/c)$^{-1}$.

4.2 $\Lambda_c \rightarrow PK\pi$ Hadronic Decay

In this section, the experimental result for the Multiplicity*Branching_Fraction is estimated for the $\Lambda_c \rightarrow PK\pi$ hadronic decay channel, where "multiplicity" means the production per event. In this dissertation the multiplicity and the particle decay processes include their charge conjugate partners unless it is stated explicitly. Since the Multiplicity*Branching_Fraction is the measured quantity, the Λ_c Multiplicity then is

extracted by using the best known BF($\Lambda_c \rightarrow PK\pi$) experimental results from other experiments. In order to observe the Λ_c signal via its PKπ decay channel, the invariant-mass distribution is constructed out of the P, K, π particles' 4-momenta and the region around the Λ_c mass ≈ 2285 MeV is studied. Numerous cuts have been applied in order to enhance the significance. The efficiency is estimated by using Monte Carlo simulated events.

The Monte Carlo simulation is composes of two stages. The first stage is responsible for the creation of the primary quarks and gluons, and also it is responsible for the following hadronization processes. The first stage also takes care of the decay processes for the short living particles (strong and electromagnetic decays). In this dissertation Jetset 5.3 computer Monte Carlo program is used where the Lund hadronization model is implemented and the $q\bar{q}$, $q\bar{q}g$, $q\bar{q}gg$, $q\bar{q}q'\bar{q}'$ primary partons creation is evaluated using the second order perturbative QCD. The Webber model was also available for the description of the hadronization processes but it has not been used extensively. The second stage of the Monte Carlo event generation is called the TPCLUND detector simulation. The inputs of this second stage are the particles' type and the momenta which are the outputs from the first stage. The comparably long living particles decay (weak decays) and the following reactions are treated in the second stage where the weak decay matrix element is used properly whenever it was needed. In this stage, when the incoming particle encounters detector material (i.e., Beam Pipe, pressure wall, IDC, field cage), then the following dominant interactions are statistically evaluated: multiple scattering, nuclear interaction, bremsstrahlung, photon conversion and dE/dx ionization energy loss. In this dissertation the "Fast Monte Carlo program" is used for the detector simulation. This Fast Monte Carlo program skips some event reconstruction details but creates statistically quite accurate final results. Since the efficiency estimation needs large number of Monte Carlo generated events, the usage of the Fast Monte Carlo is quite adequate.

4.2.1 $\Lambda_c \to PK\pi$ Selection

There are three main reasons which are responsible for the difficulty of the $\Lambda_c \to PK\pi$ decay observation. First, the Λ_c production rate per good hadronic event is low (about .05-.15). Second, the expected BF($\Lambda_c \to PK\pi$) is small (about 4.3%; see below). Third, since the Λ_c lifetime is short ($c\tau \approx 57$ micron), then it is not feasible to isolate the distinct $\Lambda_c \to PK\pi$ decay vertex in our TPC environment. All these factors cause the presence of substantial background contamination and, consequently, serve as obstacles for the Λ_c detection. Our main task is to increase the signal significance by imposing meaningful and effective cuts in an unbiased way. After some careful study the following cuts were applied:

1) The hadprob for π, K, P is required to be larger than 0.7, 0.2, and 0.15, respectively. In addition to this, if the incoming particle satisfies both the proton and kaon hadprob cut conditions, then dual identification is prescribed for that particle.

2) The scaled Λ_c candidate momentum is chosen to be larger than 0.5.

$$x_p \equiv \frac{\left|\vec{P}_{(P+K+\pi)}\right|}{P_{beam}} > 0.5 \ .$$

3) The absolute momenta of π, K, P particles are chosen to be larger than 0.4, 0.8, 3.0 GeV, respectively.

4) The vector sum of the absolute transverse momenta of π, K, and P particles relative to the Λ_c candidate momentum direction is chosen to be larger than 1.0 GeV:

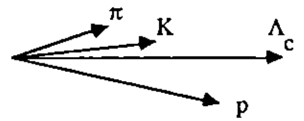

$$P_T^{SUM} \equiv |P_T^{\pi}| + |P_T^{K}| + |P_T^{P}| > 1 \text{ GeV}.$$

The scaled momentum cut is based on the characteristics of the Λ_c production mechanism. According to LUND model, the Λ_c particle is mainly produced when a primary charm quark combines with an $(ud)_0$ diquark. Since the Λ_c is much heavier than the remnant anti-diquark, the Λ_c is expected to carry a large portion of the initial charm quark momentum. According to the Monte Carlo simulation, the scaled momentum cut suppresses the background substantially while a large fraction of the Λ_c's (.57 fraction of Λ_c's when the hadprob of the P, K, and π particles are determined as above) pass this cut. This scaled momentum cut also eliminates almost all Λ_c's originating from $b\bar{b}$ events. The motivation for the hadprob cut selection is based on the fact that the protons originating from the genuine Λ_c's have an identification ambiguity. After scaled momentum cut enforcement, the proton momentum distribution falls in the range where the proton identification could be confused with the kaon identification (see Figure 3.11, 4.1(b), 4.1(c)). The fact that protons happen infrequently in the general events and specially in comparably large momentum range then it was possible to lower the hadprob cut values for the kaons and protons and allow double identity between them in order to capture more Λ_c's. The pion momentum cut is due to large pion fraction in the background events. The P_T^{SUM} cut reflects the fact that a significant amount of $Q \approx 720$ MeV residual energy is transferred into p, K, and π daughter particles. In the rest frame and for the unpolarized Λ_c particle, which is true in our case, the Λ_c's decay isotropically. But the fake Λ_c's, which are made of random combinations of p, K, and π jet constituent particles, are expected to "decay" anisotropically. In this case, the fake Λ_c momentum direction is expected to serve as a symmetry axis for the spatial distribution of the "daughter" particles.

After applying the above-mentioned cuts, the invariant mass distribution of Λ_c and $\hat{\Lambda}_c$ particles is represented in Figure 4.2. This particular set of cuts is chosen on the ground that it has an average $Signal_{data}$/Efficiency value (that is, its extracted multiplicity will be unbiased by the cuts) while the significance is at maximum. Each of the cuts used was varied around the final cut values; the extracted multiplicity were found to be stable (as one would hope, see Figure 4.6) to these variations.

Here, the averaging process is computed in 5-dimensional space: Hadprob_K and Hadprob_P, Momentum_π, Momentum_K, Momentum_P, P_T^{SUM}. If these five variables are independent, then the $Signal_{data}$/Efficiency can be represented as:

$Signal_{data}$/Efficiency =

$$\frac{\alpha_1^{data}(Hadprob\_cut)*\alpha_2^{data}(P_\pi\_cut)*\alpha_3^{data}(P_K\_cut)*\alpha_4^{data}(P_{pr}\_cut)}{\alpha_1^{MC}(Hadprob\_cut)*\alpha_2^{MC}(P_\pi\_cut)*\alpha_3^{MC}(P_K\_cut)*\alpha_4^{MC}(P_{pr}\_cut)}$$

$$*\frac{\alpha_5^{data}(P_T\_cut)*Signal_{data}(No\_cuts)}{\alpha_5^{MC}(P_T\_cut)*Signal_{MC}(No\_cuts)}*(\#\Lambda_c^{MC}(no\_cuts) =$$

$$\alpha_1(Hadprob\_cut)*\alpha_2(P_\pi\_cut)*\alpha_3(P_K\_cut)*\alpha_4(P_{pr}\_cut)*\alpha_5(P_T\_cut)\,;$$

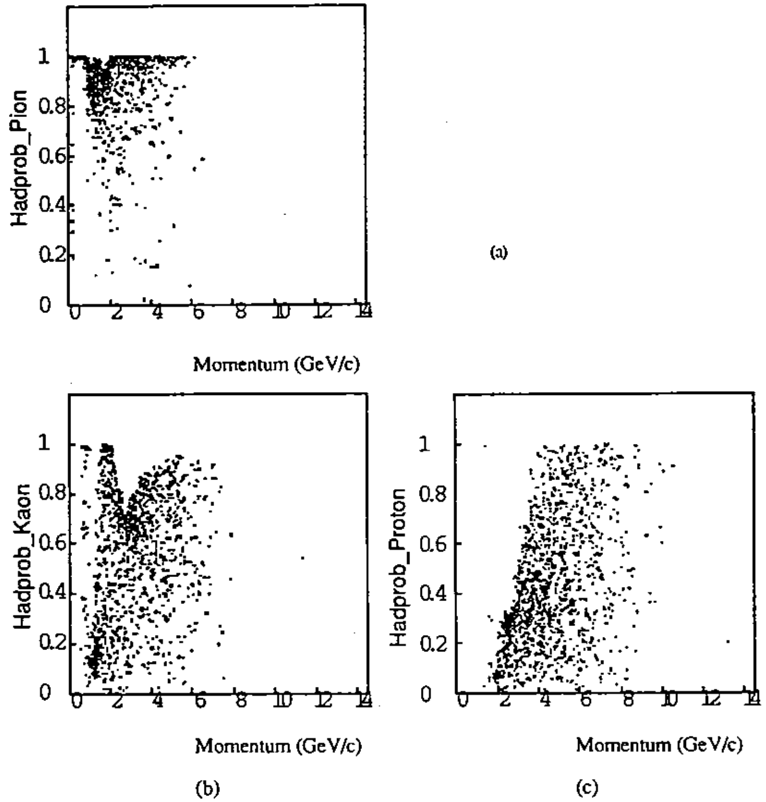

Figure 4.1. (a), (b), and (c) display Monte Carlo results for the hadprob as a function of momentum for π, k, and p particles, respectively. Here, the hadprob_pion, hadprob_kaon, and hadprob_proton are the hadron probability of π, k, p particles for being identified as π, k, and p, respectively, where π, k, p particles were decay products of true Λ_c particles. The π, k, and p particles were identified (right or wrong) on the detector level when only

x_p >0.5 the scaled momentum cut was applied. The result is based on the "Λ_c MC events" which is equivalent to 1,075,066 "Good Hadronic" MC events.

where α_1^{data}(Hadprob_cut), α_2^{data}(P_π_cut), α_3^{data}(P_K_cut), α_4^{data}(P_{pr}_cut) are attenuation factors after imposing Hadprob_cut, P_π_cut, P_K_cut, and P_{pr}_cut, respectively. The last expression implies that the formula A.1 (see Appendix) could be appropriate to be used. Therefore, the averaging algorithm for the five variables can be formulated:

$$(S/Ef)_{Ave} = (S/Ef)_{Ave\_Hpr} \cdot (S/Ef)_{Ave\_P_T} \cdot (S/Ef)_{Ave\_P_\pi} \cdot (S/Ef)_{Ave\_P_K} \cdot (S/Ef)_{Ave\_P_P} \frac{1}{(S/Ef)^4_{Start}} \quad (4.1)$$

Here, the $(S/Ef)_{Ave\_Hpr}$ is the average value of the Signal_{data}/Efficiency when the Hadprob_K and Hadprob_P cuts have been varied and the other four cut parameters were fixed to constant initial values. $(S/Ef)_{Start}$ denotes the value of Signal_{data}/Efficiency for the starting initial values of Hadprob_K&P, Momentum_π/K/P, and P_T^{SUM}. Since not all variables are completely independent, the averaging procedure has been repeated several times. This averaging procedure is applied in order to avoid accepting statistically biased (large or small) values of the Signal/Efficiency. The validity of this averaging procedure is justified by the presumption that the statistical uncertainty of the Signal_{data}/Efficiency is much larger than the unforeseen systematic uncertainties related to the Hadprob_K&P, Momentum_π/K/P, and P_T^{SUM} variables. Since the presumption mentioned above is true (see Figure 4.6) then there is no danger to obscure (to average out) the potentially interesting physical content within the signal.

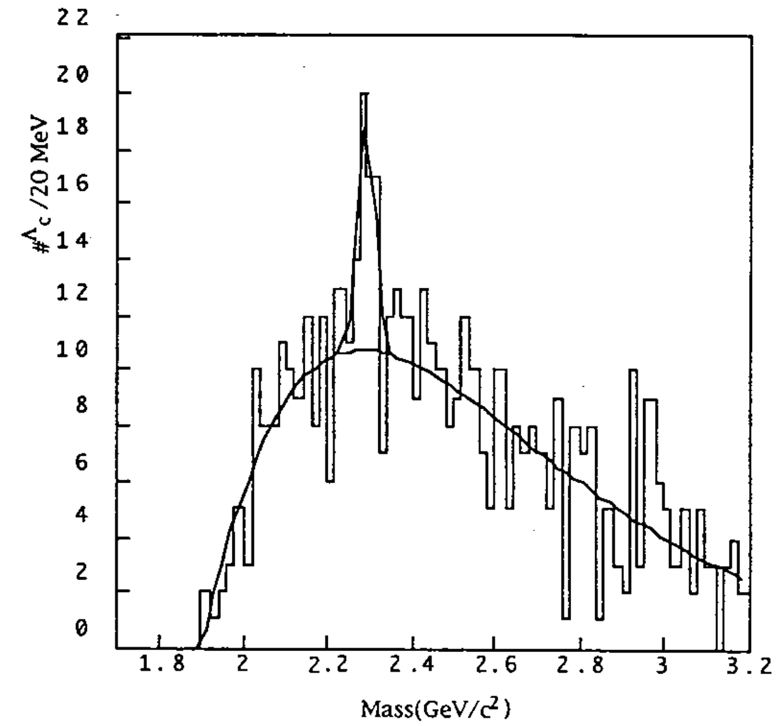

Figure 4.2 Invariant-mass distribution of $\Lambda_c \to PK\pi$ decay based on data.

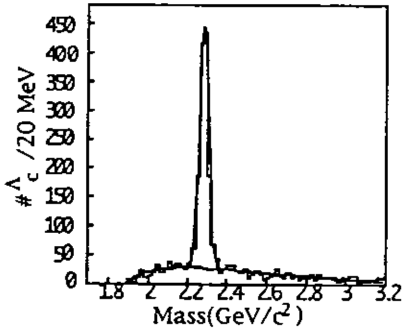

Figure 4.3 Invariant-mass distribution of $\Lambda_c \to PK\pi$ decay based on generated "Λ_c events" equivalent to $1.66*10^6$ Monte Carlo "Good Hadronic events."

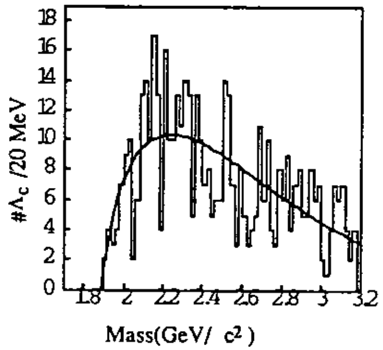

Figure 4.4 Invariant-mass distribution of wrong sign $P^+K^-\pi^-$ and $P^-K^+\pi^+$ combinations in data. No attempts were done to fit the fake Λ_c signal.

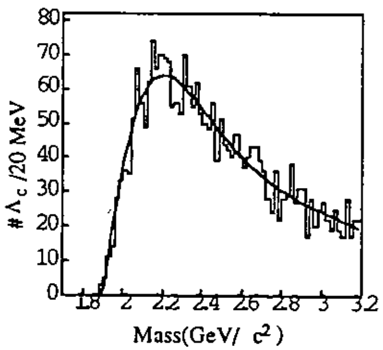

Figure 4.5 Invariant-mass distribution based on 126,730 "Good Hadronic" MC events without $\Lambda_c \to PK\pi$ source.

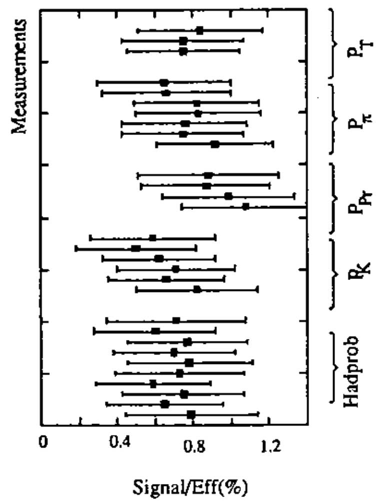

Figure 4.6 Signal/Efficiency(%) is plotted for various Hadprob_K/P, Momentum_π/K/P and P_T cuts when the initial cuts of these variables are .2/.15, .4/.8/3.0GeV, and 1.0GeV, respectively. The plot demonstrates that the Signal/Efficiency(%) variance is negligible comparing to statistical uncertainties for the following cut parameters:

Hadprob_K/P(cut) =.2/.15, .2/.2, .2/.25, .2/.3, .2/.35, .35/.15, .35/.2, .35/.25, .35/.3, .35/.35

Momentum_K (cut)= 0, 1.4, 1.6, 1.8, 2.0, 2.2

Momentum_P (cut)= 0, 2.5, 3.5, 4.0

Momentum_π (cut)= 0, .6, .8, 1.0, 1.2, 1.4, 1.6

P_T (cut) = 0, .8, 1.2

Two independent functions are used to fit the histogram depicted in Figure 4.2. One of these functions is a Gaussian function for the signal fit and the second function is the a parameter smooth function for the background fit. The RMS width of the Gaussian distribution is determined from the Monte Carlo study and is fixed at 20 MeV (see Figure 4.2, 4.3). Figure 4.3 displays the Λ_c invariant-mass distribution for the Monte Carlo generated events where each event is a regular hadronic event except that it contains a $\Lambda_c \rightarrow PK\pi$ source in it. These generated events are equivalent to $1.66*10^6$ "Good Multihadronic" events with respect to their Λ_c content. In these generated events the parent Λ_c particle decays isotropically in its rest frame. Since the Λ_c particle decays weakly, it has a negligible mass uncertainty (about 0.003 eV); thus the Gaussian width is a result of the P, K, π particles momentum measurements' uncertainties. Further Monte Carlo studies show that the RMS signal width dependence on the scaled momentum is small and, therefore, insignificant in this analysis. The background fitting function for the distribution in Figure 4.2 is chosen to be:

$$\text{Fit\_Back} = A(1+Bx + Cx^2)(D-x)^{20}x^E$$

where A, B, C, D, and E are free parameters and x=M-1.9. In generally $x=M-M_{min}$ and M_{min} is the lowest possible invariant mass of the decay product particles and in our case $M_{min}=M_P+M_K+M_\pi \approx 1.57$. The enforced P_T^{SUM} cut has shifted M_{min} value upward ≈ 1.9.

After the fitting, the combined number of observed Λ_c and $\bar{\Lambda}_c$ is 19.3 ± 7.8. This signal is peaked at M=2292±9 MeV, which is in agreement with the world average Λ_c mass (2285.2±1.2 MeV). The probability for the background (44 events) within a $\pm 2\sigma$ range of the peak to fluctuate and to become larger than the background plus signal value

(63) is less than 0.2%. When the same cuts were applied to the data but with wrong-sign $P^+K^-\pi^-$ combinations, then no observable signal was noticed around the Λ_c mass region (see Figure 4.4). Similarly, no signal was observed around the Λ_c mass for the 126,730 MC generated events where the $\Lambda_c \rightarrow PK\pi$ source was deliberately eliminated (see Figure 4.5).

x_p	Efficiency (%)	Data	Multip*BF ($x10^{-3}$)
0.5-0.6	20 (±1.4)	6.2±5.5	1.20±1.07
0.6-0.75	28 (±1.3)	9.2±5.0	1.27±0.69
0.75-1.0	33 (±2.2)	3.9±2.9	0.46±0.34
Total (x_p=0.5-1.0)		19.3 ±7.8	2.93±1.31

Table 4.1 The MC estimated efficiencies and the recorded number of Λ_c's from the data are listed for three x_p bins. The total Multiplicity*BF($\Lambda_c \rightarrow PK\pi$) is extracted from this information for the x_p=0.5-1 region.

In the Table 4.1, the data for the Λ_c&$\bar{\Lambda}_c$ combined signal is listed for three x_p bins in conjunction with the estimated Efficiency and measured Multiplicity*BF. The efficiency uncertainties are enclosed in parentheses and are treated as a part of the systematic uncertainties (see section 4.2.2 below). The result is Multiplicity*BF(x_p=0.5-1.0)=.00293±.00131(stat); this is the central experimental result of this thesis. The Figure

4.7 shows the x_p scaled momentum distribution for the Multiplicity*BF entity for the three x_p bins. On this figure only the statistical errors are shown. On the same plot also the Lund predicted Multiplicity*BF distribution is shown, normalized to the data. Clearly, the measured momentum spectrum is poorly determined; this comparison serves only to show that the measured spectrum is not wildly different from the shape expected from Monte Carlo studies. After using the x_p extrapolation coefficient=1.69 (discussed below), the Multiplicity*BF for the total x_p range of 0.0 to 1.0 becomes 0.0050±0.0022. If one uses the best known BF($\Lambda_c \to PK\pi$) =4.3±(1.1)%[1] then the overall multiplicity becomes 0.12 ±0.05(stat).

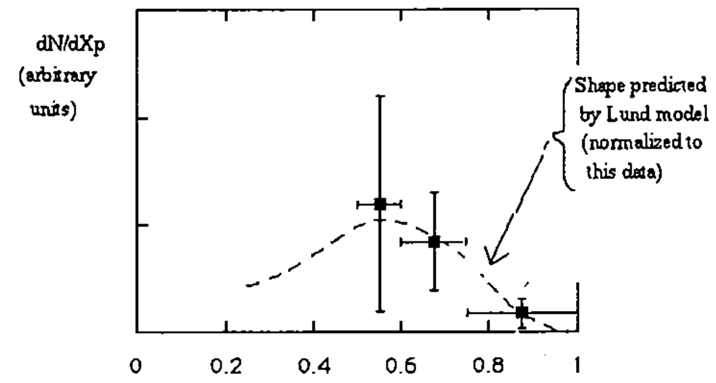

Figure 4.7 Λ_c scaled momentum distribution is shown for three x_p bins (data).

4.2.2 Λ_c Acceptance Correction and Total Cross Section for the $\Lambda_c \to PK\pi$ Decay Channel

There are several sources of systematic uncertainties which increase the uncertainty of the measured Λ_c multiplicity value. One of the major sources of systematic uncertainty is in the x_p extrapolation. Within this experimental framework, the Λ_c measurements were conducted in the limited x_p=0.5-1.0 scaled momentum region. To estimate the Λ_c multiplicity for the entire x_p=0.0-1.0 momentum region, an extrapolation coefficient must be estimated. According to the CLEO[2] result, the extrapolation coefficient extracted from their Λ_c data distribution is 1.44±.22 for x_p=0.0-1.0. The CLEO experiment was conducted at $\sqrt{S}$=10.55 GeV and the analysis did not include Λ_c contributions from the $b\bar{b}$ events. MC analyses indicate that the $b\bar{b}$ events contribute about 19% of the Λ_c's originating from the $c\bar{c}$ events at E_{cm}=29GeV and that 80% of the Λ_c's originating from the $b\bar{b}$ events have x_p<.5. If the LUND estimate of Λ_c's originating from $b\bar{b}$ events is allowed to possess a 50% uncertainty, then the x_p extrapolation coefficient including the $b\bar{b}$ events contribution becomes about 1.69±0.26 (or ±15%) at E_{cm}=29GeV. The estimated x_p extrapolation uncertainty (±0.26) required the knowledge of the uncertainty of the number of Λ_c's with x_p=0.5-1.0 which has been estimated (~10%) from the Λ_c distribution out of CLEO[3] result for PKπ channel. The absolute value of the x_p extrapolation coefficient is evaluated with LSFF parameters a=.60 (±.10±.04), b=.52 (±.05±.03) GeV^{-2} which are optimally parametrized by the CLEO[4] collaboration for the best available charmed hadron data. In the last-referenced article it was established that the LUND model's parameters once adjusted for the E_{cm}=10.55 GeV central mass energy can be used for any center of mass energy case as well (including E_{cm}=29 GeV case). This is because the momentum distribution of charmed hadrons is sensitive to QED and QCD corrections and the LUND model treats these corrections properly for the provided center of mass energy value.

The second significant contribution to the systematic uncertainties is the track finding efficiency. For any stable charged particle inside the TPC volume the track finding efficiency is estimated to be equal to 97±2%. Therefore, the uncertainty of the simultaneous track reconstruction of three daughter particles π, K, p is about 6%. The correction for tracking efficiency has already been included in the Monte Carlo estimation of the efficiency, but its uncertainty must be included in the overall uncertainty.

The third significant factor of the Λ_c multiplicity uncertainty is that due to nuclear interactions. The uncertainties related to the nuclear interactions between the hadrons and the material composing of the beam pipe and inner pressure wall (just before the TPC sensitive volume) is known according to the following:[5]

a) The nuclear interaction length is known within 10% uncertainty.

b) The total nuclear interaction rate is known within 20% uncertainty.

c) The production cross section for the specific initial and final particles case is known within 75% uncertainty.

The Monte Carlo generated events were analyzed both with and without the presence of the nuclear interaction. The detected Λ_c's increased by 20% after turning the nuclear interaction off. Therefore, total uncertainty from nuclear interaction (20%) is about 20*0.2=4%. The expected uncertainty contribution due to lack of knowledge of the precise nuclear interaction length (10% error) is $\frac{\exp(-\frac{X+\delta X}{X_o}) - \exp(-\frac{X}{X_o})}{\exp(-\frac{X}{X_o})} \approx \frac{\frac{\delta X}{X_o}}{1-\frac{X}{X_o}} \approx 2.5\%$; where

X_o is the Nuclear Interaction Length of the material and $1-\frac{X}{X_o} \approx .2$ value is used since the presence of the material attenuates the Λ_c flux by 20%. The overall expected uncertainty contribution of these two effects into the Λ_c multiplicity is about 5%. The uncertainty of the product particle composition after the nuclear interaction is irrelevant for the Λ_c multiplicity estimate.

There is also an uncertainty in the Λ_c multiplicity associated with the particle identification, in particular the error on the χ^2 parameter. The systematic uncertainties related with the particle identification are:

a) The dE/dx curve is known within .2% error.

b) The dE/dx resolution is known within 8% error.

c) The momentum resolution is known within 10% error.

Among these uncertainties, the dE/dx resolution uncertainty is the dominant one.[6] Monte Carlo generated events were analyzed with 2.9% default dE/dx resolution value. Second Monte Carlo generated events set was analyzed with the dE/dx resolution incremented by 8%. The change in the detected Λ_c rate is estimated to be roughly 4%.

The systematic uncertainty related with the signal and background fitting is estimated by imposing the following variations:

a) The Gaussian and the background shapes were fixed according to Monte Carlo.

b) The Gaussian shape was fixed according to Monte Carlo and the background was fit to the data.

c) The Gaussian and the background shapes were fit to the data.

From studying these variations, the estimated systematic uncertainty for the Λ_c multiplicity due to data fitting is estimated to be about 10%.

The final systematic uncertainty contribution is due to the limited number of Monte Carlo generated events and is about 4%. The Table 4.2 lists the summary of Λ_c multiplicity correction coefficients and their uncertainties.

Source	Correction	Uncertainty (%)
x_p Extrapolation	1.69	15
Tracking	1.00	6
Nuclear Interaction	1.00	5
Particle Identification	1.00	4
Signal and Back. Fitting	1.00	10
Monte Carlo Statistics	1.00	4
Subtotal	1.69	20

Table 4.2 Summary of the Λ_c multiplicity correction coefficients and their uncertainties.

So far the branching fraction uncertainty has not been incorporated yet. The combined systematic uncertainty of the BF($\Lambda_c \rightarrow PK\pi$) =4.3±1.1% uncertainty (about

26%) and the subtotal uncertainty (about 20%) from Table 4.2 totals about 33%. The final result for the Λ_c multiplicity becomes:

Multiplicity(Λ_c) = 0.115±0.051(stat)±0.023(syst)±0.029(syst(BF))

= 0.115±0.051(stat)±0.037(syst) = 0.115±.063(stat+syst) ≈ 0.12 ± 0.06(stat+syst).

The number of Λ_c or $\bar{\Lambda}_c$'s per charm quark can be estimated by assuming that there are 2*4/11 c or $\bar{c}$ quarks per hadronic event, and correcting for the Λ_c's above x_p=0.5 originating from $b\bar{b}$ events (about 5% of the total), and using the x_p extrapolation factor of 1.44±.22 (±15%) quoted by CLEO for $c\bar{c}$ events:

$$\frac{\Lambda_c}{c} = \frac{\text{Multip*BF}(x_p\text{=0.5-1.0})}{\frac{8}{11}\cdot \text{BF}}\frac{1.44}{1.05} = .128 \pm .063(\text{stat+syst}) \pm .033(\text{BF only})$$

$$\approx 0.13 \pm 0.07(\text{stat+syst})$$

Our measurement of the number of Λ_c per charm quark is somewhat in between the Mark II[7] and the CLEO[8]/ ARGUS[9] results, as listed in Table 4.3. The Mark II measurement for the Λ_c per charm is a direct measurement and does not use branching fraction information, but does presume that 60% of the Λ_c's will eventually decay into a proton. To be able to compare these results, the systematic uncertainty due to the branching fraction has been separated in the ARGUS and CLEO results, and in the present analysis. Our result is in agreement with the Mark II, ARGUS, and CLEO results and the differences of our result from the Mark II, ARGUS and CLEO results are less than one standard deviation. From the same Table 4.3 one may make an observation that the earliest Mark II result is significantly above the CLEO and ARGUS results. It is speculated[10] that the Mark II result contains large ambiguities which have been underestimated by the authors and therefore that Mark II result is less reliable. The weighted average of the ARGUS, CLEO, and TPC/2γ results (all of which use the PKπ decay mode and share in common its uncertainty) is Λ_c/c=0.091±0.013(stat+syst), excluding the BF($\Lambda_c \to PK\pi$) uncertainty (and ±.026 including it).

The Mark II, ARGUS, CLEO, and our measured Λ_c multiplicity values are consistently higher than the LUND, WEBBER, and UCLA predictions. The differences of our measured Λ_c multiplicity in units of standard deviations from the LUND, WEBBER, and UCLA model predictions are about 1.1, 1.3, and 1.3σ, respectively (see Table 4.4). In these estimates, the contribution of the BF($\Lambda_c \to PK\pi$) uncertainty plays a significant role and therefore we would like to approach this from a somewhat different perspective: The measured value #Lamc*BF($\Lambda_c \to PK\pi$) per charm quark is expected to be independent of e^+e^- annihilation energy; the weighted average of ARGUS, CLEO, and our TPC/2γ results is:

$$(\Lambda_c/c)BF = .00389 \pm .00055.$$

If one would use LUND estimate of $\frac{\Lambda_c}{c} = \frac{0.055}{1.19} \cdot \frac{1}{8}\frac{1}{} = .064$ then the estimated BF($\Lambda_c \to PK\pi$) becomes:

$$BF(\Lambda_c \to PK\pi) = 6.08 \pm .86\% \approx 6.1 \pm .9\%$$

Group	Date	BF(%) Presumed	(Λ_c/c) BF $*10^{-3}$	Λ_c/c
Mark II (SPEAR) 5.2 GeV	1-1980	--------		.20±.05(stat+syst)
ARGUS 10.2 GeV	6-1988	4.3±1.1	3.66±.72(stat+syst)	.085±.017(stat+syst) ±.022(BF only)
CLEO 10.5 GeV	9-1990	4.3±1.1	4.07±.88(stat+syst)	.095±.020(stat+syst) ±.024(BF only)
TPC/2γ, 29 GeV (present analysis)	5-1992	4.3±1.1	5.53±2.71(stat+syst)	.13±.06(stat+syst) ±.03(BF only)
Combined ARGUS, CLEO, and TPC/2γ results			3.89±.55(stat+syst)	.091±.013(stat+syst) ±.023(BF only)

Table 4.3 Measurements of the number of Λ_c's per charm quark according to Mark II, ARGUS, CLEO, and the present TPC/2γ experiment based on $\Lambda_c \to PK\pi$ data.

Measured Multiplicity	Lund	Deviation (# Sigma)	Webber	Deviation (# Sigma)	UCLA	Deviation (# Sigma)
.12±.06	.055	1.1	.042	1.3	.04	1.3

Table 4.4 The predicted Λ_c multiplicity values according to the Lund, Webber, and UCLA models and their deviations from the measured Λ_c multiplicity in units of standard deviations (σ).

This is 2.1 standard deviation above the present experimental value of BF($\Lambda_c \rightarrow PK\pi$) = 4.3± 1.1% (excluding its uncertainty from the comparison). The WEBBER and UCLA models yield results of 8.0%±1.1% and 8.5±1.2%, 3.4 and 3.5 standard deviations above the present experimental value. Therefore, from this analysis we may conclude that there is a strong evidence that:

a) BF($\Lambda_c \rightarrow PK\pi$) is larger than 4.3% and/or

b) The Λ_c multiplicity is larger than the present models predict.

If we presume the validity of BF($\Lambda_c \rightarrow PK\pi$) = 4.3± 1.1%, then Mark II, ARGUS, CLEO, and our measured Λ_c multiplicity results suggest the possibility that perhaps the color dynamics in the vicinity of a heavy quark (charm and heavier) is different than the for light quark case. There is a speculation[11] which suggests that the colorfield density could be condensed in the heavy quark vicinity. This is because the heavy quarks are localized (have low mobility) in space and time while they exchange gluons with neighbor quarks. The larger colorfield strength around the heavy quark could enhance the baryon production rate. This scenario corresponds to an increase of the string tension (k) in Formula 2.6 for the LUND model case or the decrease of the b parameter value in Formula 2.10 for the UCLA model case. In this case, the k coefficient in Formula 2.6 needs to be interpreted as a tension of the colorfield tube per unit cross-section area.

4.3 $\Lambda_c \rightarrow P\overline{K^o}$ Hadronic Decay

Despite the fact that the branching fraction[12] for the $\Lambda_c \rightarrow P\overline{K^o}$ hadronic decay is relatively small (2.1 ±0.6%), it is tempting to explore this channel since it has a low background level. The K^o meson (the antiparticles behave in similar fashion) can be represented as a combination of K^o_S and K^o_L CP eigenstates each with equal weight. The K^o_S particles have a mean life time $c\tau$ = 2.675 cm and decay into $\pi^+\pi^-$ with a 68.6% branching fraction. A standard TPC/2γ secondary vertex finding algorithm has been developed in order efficiently to find the K^o_S particles. The K^o_S finding algorithm uses only the $K^o_S \rightarrow \pi^+\pi^-$decay channel. The detailed description of the K^o_S finding algorithm is discussed elsewhere.[13] According to this K^o_S secondary vertex finding algorithm, the K^o_S must be rejected if the $\pi^+\pi^-$ daughter particles' dE/dx information and kinematics are consistent with either e^+e^- photon conversion or $\Lambda \rightarrow \pi p$ decay. The K^o_S is also rejected if the reconstructed secondary vertex point originates from the region where the TPC/2γ detector's cylindrical walls are located and if the "deflection angle" is greater than 10°. The deflection angle is the angle between the vector of K^o_S parent particle momentum direction and the vector joining the primary vertex and the secondary vertex. The "wall rejection" algorithm rejects those K^o_S's which result from nuclear interaction between the incoming hadron and the nucleon of the nucleus of a wall atom. Finally, if there are secondary vertices sharing the same track then among these secondary vertices the one which has the best "secondary vertex quality" will be accepted.

The cuts for this $\Lambda_c \rightarrow P\overline{K^o}$ decay channel are the followings:

a) Hadprob for the proton should be at least 0.15.

b) The scaled Λ_c momentum must be at least 0.5.

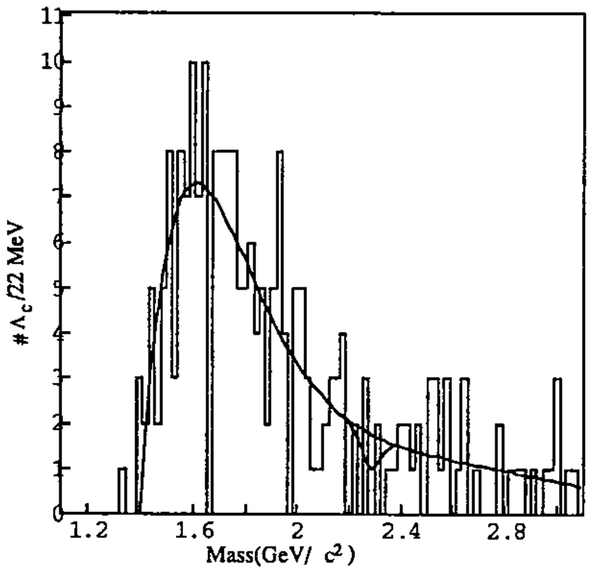

Figure 4.8 Invariant-mass distribution of $\Lambda_c \rightarrow P\overline{K}^0$ decay based on data.

After applying these cuts, the Monte Carlo estimated acceptance (not including the branching fraction) for the $\Lambda_c \rightarrow P\overline{K}^0$ decay channel becomes 6.3±0.5%. The resulting invariant-mass distribution of $P\overline{K}^0$ combinations is shown in Figure 4.8. The histogram is fit by a five parameter polynomial function for the background and Gaussian function for the signal. The RMS width (standard deviation) of the Gaussian function is fixed at 35 MeV, as determined by Monte Carlo. From the fitting, the signal is -3.0± 3.0 events. During the fitting the center of the Gaussian curve was fixed at the 2285 MeV expected Λ_c

mass. Since the signal is small, only the estimated upper limit can be meaningful. Nowadays in the scientific community several methods are used to estimate the upper limit. The estimated upper limit value and its interpretation depend highly on the particular method in use. In this dissertation only the "Poisson processes with background" method[14] is used. This method is equally valid for large and small statistics. This method also is independent of the signal shape and presumes that the errors of the expected background and the expected center of the peak area are negligible.[15] The upper limit of the recorded signal (-3.0± 3.0) at 90% Confidence Level for the known background $n_B \approx 10$ (evaluated from the data within $M(\Lambda_c) \pm 2\sigma$ invariant-mass range) is equal to 5. By using the acceptance value (≈6.3%), and presuming the most recent and reliable branching fraction value (2.1±0.6, see above for the reference) for the $P\overline{K}^0$ decay then the upper limit with 90% Confidence Level for the Λ_c production rate per hadronic event becomes 0.15. For this upper limit estimate the acceptance correction or branching fraction correction has not been incorporated since they do not affect the relationship between the background and number of observed events within the region of interest. Thus the production rate of Λ_c's per hadronic event based on $\Lambda_c \rightarrow P\overline{K}^0$ decay channel becomes:

$$\text{Multiplicity}(\Lambda_c) = -.088 \pm .091 < .15 \ (90\% \text{ CL})$$

4.4 $\Lambda_c \rightarrow P\overline{K}^0 \pi^+\pi^-$ Hadronic Decay

The cuts for this $\Lambda_c \rightarrow P\overline{K}^0 \pi^+\pi^-$ hadronic decay channel are:

a) P, $\overline{K}^0$ are defined as in the $\Lambda_c \rightarrow P\overline{K}^0$ decay analysis (see Section 4.3).

b) Protons' Hadprob value must be at least 0.7.

c) x_p scaled momentum must be at least 0.5.

After applying these cuts the Monte Carlo estimated acceptance for the $\Lambda_c \to P\overline{K}^0 \pi^+\pi^-$ hadronic decay channel becomes 6.3± 0.6%. The data for the invariant-mass distribution of $\Lambda_c \to P\overline{K}^0 \pi^+\pi^-$ is shown on Figure 4.9. The fitting on this distribution is enforced at 2285 MeV fixed Λ_c mass and with fixed 20 MeV RMS width. After fitting, the estimated signal is 5.4±8.9. Since the signal is small, only the estimated upper limit can be meaningful. The upper limit of the recorded signal (5.4±8.9) at 90% Confidence Level for the known background n_B≈66 (evaluated from the data within $M(\Lambda_c) \pm 2\sigma$ invariant-mass range) is equal to 20. By using the acceptance value (≈6.3%) and presuming the most recent and reliable branching fraction value (1.8±.6%) for the $P\overline{K}^0 \pi^+\pi^-$ decay, the upper limit with 90% Confidence Level for the Λ_c production rate per hadronic event becomes 0.7. (Note: One may get a fairly close upper limit value (≈.57) for the Λ_c production rate if one would use the standard algorithm $X_{UL}=X_m+1.28*\sigma$ which is valid for the Gaussian statistics). Thus the production rate of Λ_c's per hadronic event based on $\Lambda_c \to P\overline{K}^0 \pi^+\pi^-$ decay channel becomes:

Multiplicity(Λ_c)= .18±.30 < .70 (90% CL).

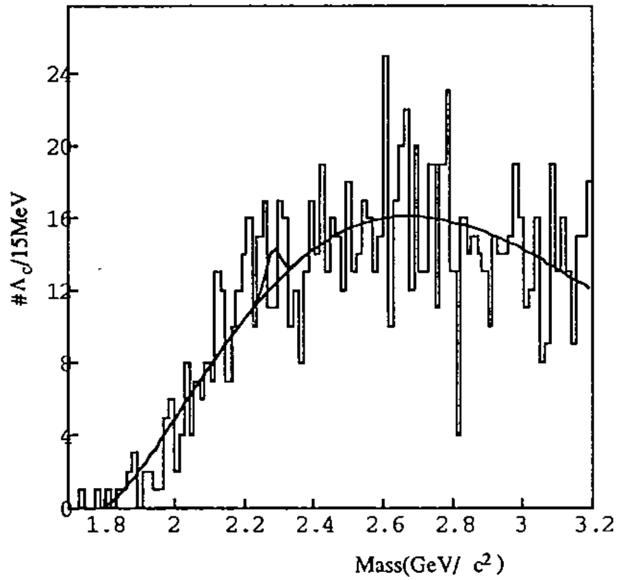

Figure 4.9 Invariant-mass distribution of $\Lambda_c \to P\overline{K}^0 \pi^+\pi^-$ decay based on data.

4.5 $\Lambda_c^+ \to \Lambda\pi^+\pi^+\pi^-$ Hadronic Decay

The detailed description of the Λ finding algorithm is discussed in elsewhere.[16] The secondary vertices of the Λ particles are determined according to the standard TPC/2γ secondary vertex finding algorithm. In this algorithm the Λ particles are determined in the same fashion as K_S^0's except with some modifications of certain numerical parameters.

The cuts for $\Lambda_c^+ \to \Lambda\pi^+\pi^+\pi^-$ decay channel are:

a) Pion's Hadprob values must be at least 0.7.

b) The scaled Λ_c momentum must be at least 0.5.

After these cuts the Monte Carlo acceptance for the $\Lambda_c^+ \to \Lambda\pi^+\pi^+\pi^-$ decay channel becomes 8.0±0.9%. The data for the invariant-mass distribution of $\Lambda 3\pi$ is represented in Figure 4.10. The fitting on this distribution is enforced at 2285 MeV fixed Λ_c mass and with fixed 20 MeV RMS width determined by MC. After fitting, the estimated signal is 10.9±8.2. Since the signal is insignificant, only the estimated upper limit can be meaningful. The upper limit of the recorded signal (10.9±8.2) at 90% Confidence Level for the known background n_B=52 (evaluated from the data within $M(\Lambda_c)\pm 2\sigma$ invariant-mass range) is equal to 18. By using the acceptance value (≈8.0%), and presuming the most recent and reliable branching fraction[17] value (2.8±.9%) for the $\Lambda\pi^+\pi^+\pi^-$ decay then the upper limit with 90% Confidence Level for the Λ_c production rate per hadronic event becomes 0.31. (Note: One may get a fairly close upper limit value (≈.37) for the Λ_c production rate if one would use the standard algorithm $X_{UL}=X_m+1.28*\sigma$ which is valid for the Gaussian statistics). Thus the production rate of Λ_c's per hadronic event based on $\Lambda_c^+ \to \Lambda\pi^+\pi^+\pi^-$ decay channel becomes equal to:

Multiplicity(Λ_c)= .19±.15 < .31 (90% CL).

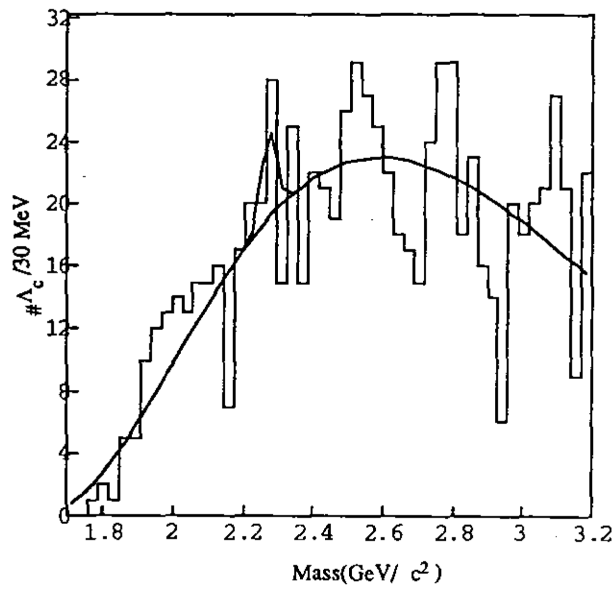

Figure 4.10 Invariant-mass distribution of $\Lambda_c^+ \to \Lambda\pi^+\pi^+\pi^-$ decay based on data.

4.6 $\Lambda_c \to e\Lambda\nu_e$ Semileptonic Decay

In this section the upper limit on the Λ_c production is estimated by reconstructing $e\Lambda$ invariant-mass combinations and using BF($\Lambda_c \to e\Lambda X$)=1.6±.71(stat+syst), the best available experimental result.[18] To avoid possible misinterpretation, it is worth mentioning that the weighted average BF($\Lambda_c \to PK\pi$)=4.3±1.1% value of ARGUS and CLEO experimental results has been used in order to evaluate the above mentioned $\Lambda_c \to e\Lambda X$

decay branching fraction. By reviewing the existing hadrons one may make a conclusion that only the Λ_c^+ particle may contain $e^+\Lambda$ right sign combinations as a final product. The possible candidates for $\Lambda_c \rightarrow e\Lambda X$ decays are: $\Lambda e\nu$, $\Sigma^0 e\nu$, $\Sigma^{*0} e\nu$, $\Lambda\pi^0 e\nu$, $\Lambda(\pi\pi)^0 e\nu$, and $\Lambda^* e\nu$. Among these, the reactions $\Sigma^0 e\nu$, $\Sigma^{*0} e\nu$, $\Lambda\pi^0 e\nu$ are highly suppressed.[19] This is because the Λ_c has Isospin=0 and the isospin carrier $(ud)_0$ diquark participates merely as a spectator during the decay reaction while any of the Σ^0, Σ^{*0}, π^0 product particles is in an Isospin=1 state. The decay modes, such as $\Lambda_c \rightarrow \Lambda(\pi\pi)^0 e\nu$, require $q\bar{q}$ quark pair creation and are highly suppressed too. This is because the required $q\bar{q}$ pair is more likely to be created between the strange quark and the $(ud)_0$ diquark due to the strong "kick" to the strange quark as a result of the large energy release during the charm quark decay. In this case the Λ as a final decay product may not exist. The $\Lambda_c \rightarrow \Lambda^* e\nu$ decay mode is suppressed[20] due to less available momentum phase space and relatively low $\Lambda^* \rightarrow \Sigma^0\pi^0$ branching fraction. Therefore, the $e\Lambda$ observation is mainly due to $\Lambda_c \rightarrow e\Lambda\nu$ decay mode. The following two arguments make the $\Lambda_c \rightarrow e\Lambda X$ observation feasible. First, since the massive Λ particle carries a substantial fraction of the Λ_c parent particle energy-momentum, then the reconstructed invariant-mass distribution of Λe particles does not spread too much (See Figure 4.14). Second, the Λ_c parent particles have a hard momentum distribution and therefore a large momentum cut (x_p>0.4) substantially reduces the background noise while substantially passing the signal. The particles are defined as in the section 4.5. In addition, the electron is required not to originate from a pair conversion. In order to get the maximum signal significance the following cuts were applied:

a) Electron Hadprob value must be at least 0.05.

b) The scaled momentum of Λe particles must be at least 0.4.

c) $P_T^{Sub} \equiv |\vec{P}_T^{c} - \vec{P}_T^{\Lambda}| = 2|P_T^{\Lambda}| > 0.5$ GeV

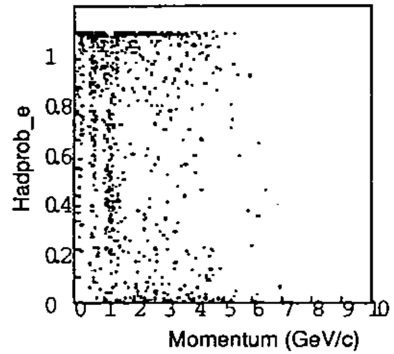

Figure 4.11. Hadron probability vs momentum of electron for being identified as an electron . Here the electron is a decay product of a true Λ_c and was qualified as a "good" track. This result is based on Monte Carlo events.

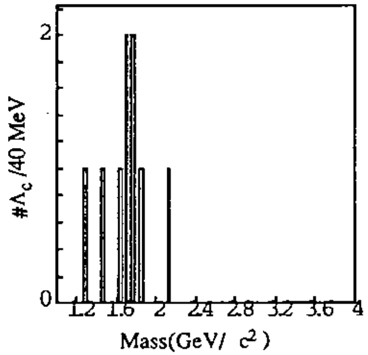

Figure 4.12 Invariant-mass distribution of right sign Λe^- and Λe^+ combinations in 126,730 "Good Hadronic" MC events where there is no $\Lambda_c \rightarrow e\Lambda\nu_e$ source.

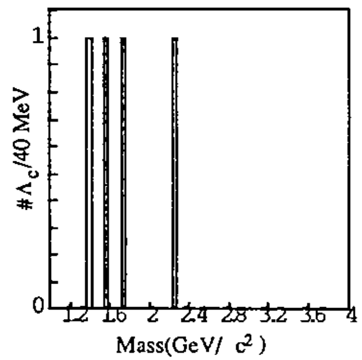

Figure 4.13 Invariant-mass distribution of $\Lambda_c \rightarrow e\Lambda\nu_e$ decay based on data.

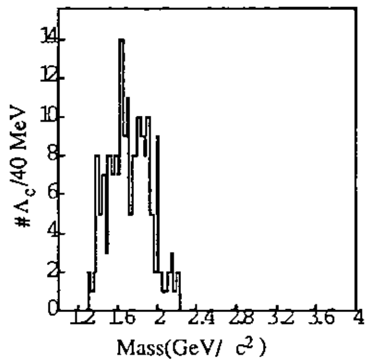

Figure 4.14 Invariant-mass distribution of $\Lambda_c \rightarrow e\Lambda\nu_e$ decay

based on generated "Λ_c events" equivalent to $1.10*10^6$ Monte Carlo "Good Hadronic events".

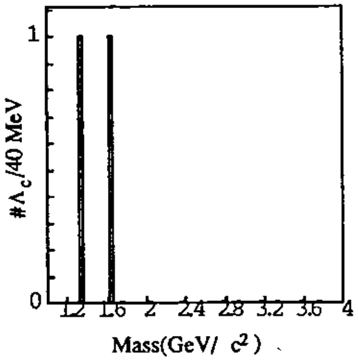

Figure 4.15 Invariant-mass distribution of wrong sign Λe^+ and Λe^- combinations in data.

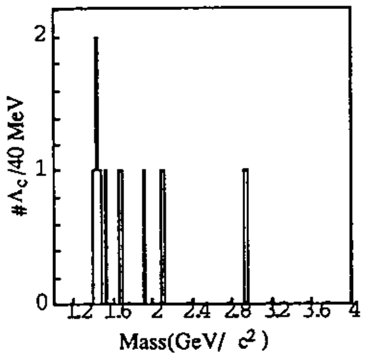

Figure 4.16 Invariant-mass distribution of wrong sign Λe^+ and Λe^- combinations in 126,730 "Good Hadronic" MC events.

After applying these cuts the overall detection acceptance of $\Lambda_c \rightarrow e\Lambda\nu_e$ decay is about 5.1±0.4%. This acceptance has been estimated by using generated Monte Carlo events where each event contains a $\Lambda_c \rightarrow e\Lambda\nu_e$ source in it. These generated Monte Carlo events are equivalent to $1.10*10^6$ "Good Multihadronic" events. The Monte Carlo program implements the weak decay matrix element for the $\Lambda_c \rightarrow e\Lambda\nu_e$ decay and that the spectator diquark collapses to a Λ particle by fusing with a strange quark. The efficiency is

determined by the ratio of the number of detected Λ_c's over the number of source Λ_c's in the generator level. While choosing the optimal cuts for the maximum signal significance, care has been taken so that $\frac{(R-W)_{data}}{Eff}$ has an average value and also that the data background level is close to its expected value (estimated by Monte Carlo study). Figure 4.13, 4.15 display the final results for the right sign $e\Lambda$ distribution (5 entries) and wrong sign $e\Lambda$ distribution (2 entries), respectively. The data entries obey Poisson statistics and the probability for a known background of 2 events to fluctuate and become larger or equal to the observed 5 events is less than 6%. For the measured signal+background value (5) with the known background (2), the upper limit at 90% Confidence Level is 7.5. Again, the "Poisson processes with background" method[21] was used in order to estimate the upper limit on the signal. By using the acceptance value (≈5.1%), and presuming the most recent and reliable branching fraction value (1.6±.71, see above for the reference) for the $\Lambda_c \rightarrow e\Lambda X$ decay, the upper limit with 90% Confidence Level for the Λ_c production rate per hadronic event becomes .36. Thus the production rate of Λ_c's per hadronic event based on $\Lambda_c \rightarrow e\Lambda\nu_e$ decay channel becomes:

$$\text{Multiplicity}(\Lambda_c) = .14 \pm .14 < .36 \text{ (90\% CL)}.$$

References

1 P.Avery et al., CLNS 90/992, CLEO 90-5, June 1990.

2 P.Avery et al., CLNS 90/992, CLEO 90-5, June 1990.

3 P. Avery et al., Phys. Rev. **D43**, 3599, (1991).

4 D. Bortoletto et. al., Phys. Rev. D37, 1719, (1988).

5 G.D. Cowen, LBL-24715, PhD Thesis, University of California, Berkeley (1988).

6 D. A. Crane, "Strange Meson Production and an Upper Limit on the Production of a Glueball Candidate in Electron-Positron Annihilation at 29 GeV", PhD Thesis, The Johns Hopkins University, (1988), JHU-HEP-88-1002

6 Review of Particle Properties, Physics Letters, **239B**, (1990).

7 G.S. Abrams et al., Phys. Rev. Lett. **44**, 10, (1980).

8 P.Avery et al., CLNS 90/992, CLEO 90-5, June 1990.

9 P.Avery et al., CLNS 90/992, CLEO 90-5, June 1990.

10 S. R. Klein, "Charmed Baryons: A new laboratory for charm studies", (1989), BU-HEP-89-16.

11 B. Anderson, G. Gustafson and T. Sjöstrand, Nuclear Phys.; **B197**, 45 (1982).

12 P. Avery et al., Phys. Rev. **D43**, 3599, (1991).

13 D. A. Crane, Ph. D. Thesis, The Johns Hopkins University, JHU-HEP- 88-1002.

14 Review of Particle Properties, Physics Letters, **239B**, (1990).

15 O. Helene, "Determination of the Upper Limit of a peak area", IFUSP-P-832, (1990).

16 J. Y. Oyang, "Inclusive Production and Flavor Corrections of Strange Baryons in e^+e^- Annihilation at $\sqrt{S} = 29$ GeV", (1991), UCLA-UEP-91-005.

17 P. Avery et al., Phys. Rev. D43, 3599, (1991).

18 H. Albrecht et al., DESY 91-055, ARGUS collaboration, (1991).

19 S. R. Klein, PhD Thesis, "Charmed and Strange Baryon Production in 29 GeV Electron Positron Annihilation", SLAC-330, (1988).

20 H. Albrecht et al., DESY 91-055, ARGUS collaboration, (1991).

21 Review of Particle Properties, Physics Letters, **239B**, (1990).

Chapter 5. Σ_c Search

5.1 $\Sigma_c \to \Lambda_c\pi$ Decay

We have also carried out searches for Σ_c's which decay via strong interaction into $\Lambda_c\pi$ particles with 100% branching fraction. The Σ_c particle is the Isospin=1 partner of the Λ_c baryon. The Σ_c's contain a c quark and two light quarks in a Spin=1, Isospin=1 state. The three isospin states of Σ_c's are Σ_c^{++}, Σ_c^{+}, Σ_c^{0} and they are expected to occur with equal rates in e^+e^- annihilation. Among these Σ_c's only Σ_c^{++} and Σ_c^{0} and their charge conjugates are observable within our experimental framework. In order to search for Σ_c's, the selection of Λ_c particles were proceeded by considering only the dominant $\Lambda_c \to PK\pi$ channel with the same selection rules as described in section 4.2.1 (except that the scaled momentum cut now is applied on Σ_c's). No cut has been enforced on the Σ_c's daughter pion except that the hadprob_π must be larger than 0.7. The distribution of inv_mass(Σ_c) - inv_mass(Λ_c) is preferred in order to suppress the measured Λ_c mass uncertainty contribution. The Λ_c candidates were chosen within inv_Mass(Λ_c)=2285±40 MeV (i.e., Mass(Λ_c)±2σ) and the resulting $\Delta m(\Sigma_c\text{-}\Lambda_c)$ distribution is displayed on Figure 5.2. The Monte Carlo estimated acceptance of Σ_c's is 11.1±1.1%. After applying the fit on the inv-mass distribution with fixed RMS width σ=4 MeV and the background shape determined by the Monte Carlo study then the measured peak area becomes 5.9±3.2. The $\Delta m(\Sigma_c\text{-}\Lambda_c)$ is estimated to be 167±2 MeV and it is in agreement with ARGUS[1] and CLEO[2] results of 167.8±0.4MeV and 167.6±1.6MeV, respectively. The upper limit on the detected signal (5.9±3.2) at the 90% Confidence Level for the known background $n_B \approx 4.3$ (estimated mean background events for the $\Delta m \pm 2\sigma$ invariant-mass region based on data) is equal to

11. By using the Σ_c acceptance value (=11.1%), and presuming the most recent and reliable branching fraction value (4.3±1.1%, see section 4.2) for the $\Lambda_c \to PK\pi$ decay and 100% for the $\Sigma_c \to \Lambda_c\pi$ decay, then the upper limit with 90% Confidence Level for the Σ_c production rate per hadronic event becomes 0.13 where this upper limit value also takes into account the contribution from the Σ_c^+ with the expectation that Σ_c^+'s contribute 1/3 of the overall Σ_c signal. The ratio of Σ_c^{++} and Σ_c^{0} particles overall multiplicity over the Λ_c multiplicity becomes equal to:

$$\frac{\text{Multiplicity}(\Sigma_c^{++} + \Sigma_c^{0})}{\text{Multiplicity}(\Lambda_c)} = 0.40 \pm 0.29 < 0.74 \text{ (90\% CL)}.$$

Again, the "Poisson processes with background" method is used in order to estimate the upper limit at 90% CL. Though the multiplicity ratio result above is not statistically very significant, it is in agreement with ARGUS and CLEO results (.24±.11 and .12±.04, respectively). Thus presuming that Σ_c^{++}, Σ_c^{+}, and Σ_c^{0} are produced with equal rates, then the fraction of Λ_c's which are decay products of Σ_c's is 0.60±0.42. We note that the ratio to Σ_c production to Λ_c production could serve as a direct way to measure the suppression of $(ud)_1$ diquark to $(ud)_0$ diquark.

The distributions of Σ_c^{++} and Σ_c^{0} particles are shown on Figures 5.4 and 5.5, respectively. There is no indication that there is any noticeable isospin mass-splitting. There are several theoretical speculations[3] that the mass differences between Σ_c^{++} and Σ_c^{0} may range[4] as much as +18 MeV to -6.5 MeV. The isospin mass-splitting may arise if the mass-energy contribution from the Coulomb static electromagnetic interaction between the quarks differs from the intrinsic mass contribution of u, d quarks (i.e., $2m_d$ versa $2m_u$). It is a mystery that so far no any experimental group has discovered Σ_c^{*} particles which have

Spin=3/2 and similar quark content as Σ_c's. According to the Lund Monte Carlo prediction the production rate of Σ_c^*'s is twice as large as the Σ_c production rate (see Figure 5.1).

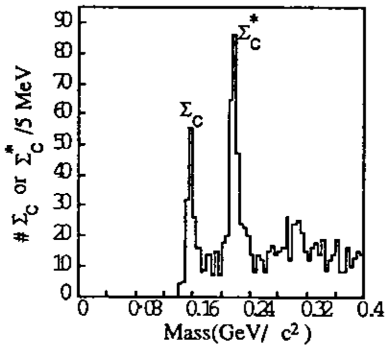

Figure 5.1 Monte Carlo study of the Invariant-mass distribution of $\Sigma_c \to \Lambda_c \pi$ decay where $\Lambda_c \to PK\pi$ with 100% branching fraction. The distribution is based on the generated "Λ_c events" (i.e., each event contains at least one Λ_c with BF($\Lambda_c \to PK\pi$)=100%) equivalent to $1.66*10^6$ Monte Carlo "Good Hadronic Events."

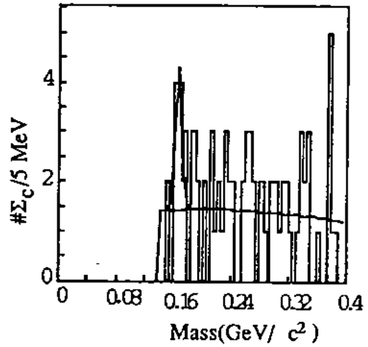

Figure 5.2 Invariant-mass distribution of Σ_c^{++} and Σ_c^0 particles from data.

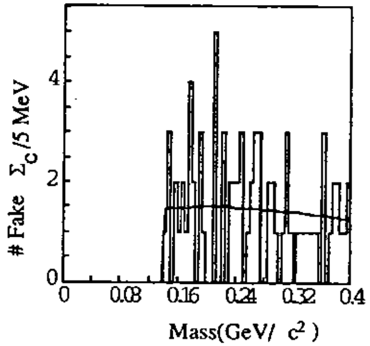

Figure 5.3 Invariant-mass distribution of fake Σ_c^{++} and Σ_c^0 particles when wrong-sign pions were used in $\Lambda_c \to PK\pi$ decay reconstruction. The distribution is based on data.

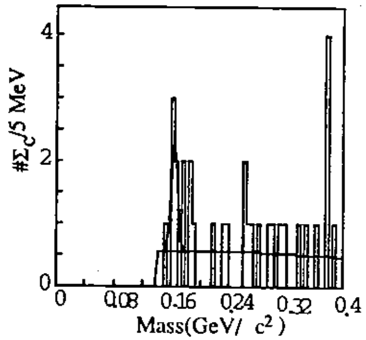

Figure 5.4 Invariant-mass distribution of Σ_c^{++} particles based on data.

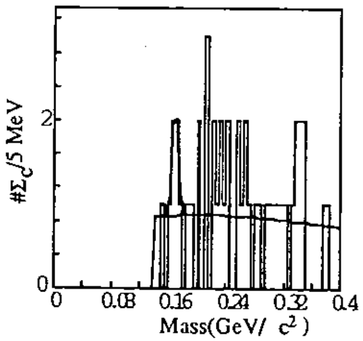

Figure 5.5 Invariant-mass distribution of Σ_c^0 particles based on data.

References

[1] H. Albrecht et al., Phys Lett. 211B, 489 (1988).

[2] T. Bowcock et al., preprint CLNS 88/876 (1988).

[3] K. Lane and Itoh et al., Progr. Theor. Phys. 54, 908 (1975);

S. Weinberg, Phys. Rev. Lett. 37,717 (1976);

L. H. Chan, Phys. Rev. D 31, 204 (1985);

S. Capstick, Phys Rev. D 36, 2800 (1987).

[4] T. Bowcock et al., preprint CLNS 88/876 (1988).

Chapter 6. Conclusions

In this experiment which uses the powerful particle identification ability of the TPC/2γ detector at PEP, Λ_c's were observed for the first time via the exclusive $\Lambda_c \rightarrow PK\pi$ decay channel at 29 GeV annihilation energy. We obtain a signal of 19.3±7.8 events. Our measured Λ_c multiplicity per hadronic event is .12±.05(stat)±.04(syst), presuming the branching fraction $\Lambda_c \rightarrow PK\pi$ is 4.3±1.1% and including its uncertainty in the quoted systematic uncertainty. This yields a value of Λ_c/c-quark of 0.13±0.07, which supports the ARGUS and CLEO results, which also use the $\Lambda_c \rightarrow PK\pi$ decay mode. The weighted average of ARGUS, CLEO, and our results for the number of Λ_c's per charm quark is estimated to be (see Table 4.3):

$$\Lambda_c/c \text{ (weighted average)} = .091 \pm .013 \text{(stat+syst)} \qquad (6.1)$$

where the branching fraction uncertainty for the $\Lambda_c \rightarrow PK\pi$ decay is discarded for a moment. The deviations of the weighted average Λ_c/c from the LUND, WEBBER, and UCLA model predictions are ~2.1-3.6 standard deviations. Hence, there is strong evidence that the branching fraction for the $\Lambda_c \rightarrow PK\pi$ decay is higher than 4.3% and/or the Λ_c multiplicity is larger than the present model predictions. If the LUND, WEBBER, and UCLA model predictions for the Λ_c production rate (which cluster around .05) are close to the true value, then the branching fraction value is determined to shift upwards from its present 4.3% value to ~6-8.5%. If, on the other hand, we presume the validity of the BF($\Lambda_c \rightarrow PK\pi$)≈ 4.3±1.1% value, then the LUND, WEBBER, and UCLA model predictions for the Λ_c multiplicity are all low by a factor of ~2. A relatively higher Λ_c production rate suggests that there might be a unique behavior of the color dynamics in the heavy quark (charm and beyond) vicinity where the color field is perhaps more condensed and therefore could cause the enhancement of the baryon production.

Mode	Signal	BF (%) (Experiment)	Multiplicity. or U.L.(90% CL)	$\frac{1}{\sigma_i^2}$	Mult* $\frac{1}{\sigma_i^2}$	χ_i^2	BF(%) (Theory)
$PK\pi$	19.3±7.8	4.3±1.1	.12±.06	277	33.2	.83	7
$P\bar{K}^o$	-3.0±3.0	2.1±0.6	-.09±.09 <.15	121	-10.7	3.37	3
$P\bar{K}^o\pi\pi$	5.4±8.9	1.8±0.6	.18±.30 <.70	11	2.0	.11	3
$\Lambda\pi\pi\pi$	10.9±8.2	2.8±0.9	.19±.15 <.31	44	8.4	.55	4
$\Lambda e\nu$	5 right sign 2 wrong sign	1.6±0.7	.14±.14 <.35	51	7.1	.19	1.9
Total				504	40	5.05	

Table 6.1 The summary list of the observed signals, branching fraction values, and multiplicities of the $PK\pi$, $P\bar{K}^o$, $P\bar{K}^o\pi\pi$, $\Lambda\pi\pi\pi$, and $\Lambda e\nu$ channels. The terms which determine the weighted average multiplicity and the reduced χ^2 values are listed as well.

The observed Λ_c mass is 2292±9 MeV and it is in agreement with the world average Λ_c mass (2285±1.2 MeV). Our extracted Λ_c momentum distribution is poorly

determined, but is in agreement with the shape predicted, for example, by the Lund model. The CLEO collaboration has parametrized their data for Λ_c momentum distribution and they concluded that the LUND Monte Carlo is fairly adequate for the description of the Λ_c momentum distribution. The UCLA model would be similar. The WEBBER model predicts a much softer Λ_c momentum distribution and it is not an adequate model to be used for the presentation of the Λ_c momentum distribution.

In Chapter 4 the Λ_c multiplicity has also been estimated by studying three addition hadronic decay channels ($P\bar{K}^o$, $P\bar{K}^o\pi^+\pi^-$, $\Lambda\pi^+\pi^-\pi^+$) and one semileptonic decay channel ($\Lambda e\nu$). The theoretical estimates of the hadronic and semileptonic decay branching fractions are within the reasonable ranges (see Table 6.1 and also sections 2.4.1 and 2.4.2). As a reminder, the hadronic decay branching fractions are based on the statistical model and it does not guarantee the accuracy better than factor of two. The additional four modes are considerably less well determined than the $PK\pi$ mode, but are in adequate agreement with it. The best estimated multiplicity value is the weighted average of these five measured multiplicity values and it is equal to:

$$\bar{n}(\Lambda_c) = \frac{\sum_{i=1}^{5} \frac{1}{\sigma_i^2} n_i}{\sum_{i=1}^{5} \frac{1}{\sigma_i^2}} = .079\pm.045(\text{stat+syst}) \tag{6.2}$$

where n_i stands for the multiplicity for the channel i (see Table 6.1). The reduced χ^2 (~5.05/4 =1.26) indicates that overall the agreement of these modes is satisfactory, despite the low value from $P\bar{K}^o$. However, we feel that the result from $PK\pi$ mode only (Λ_c multiplicity=0.12±.06) is the more conservative result to quote and use from our studies.

There is an indication of a Σ_c signal of 5.9±3.2 events. Our measured $\Delta m(\Sigma_c - \Lambda_c)$ is estimated to be equal 167±2 MeV and it is in agreement with ARGUS and CLEO results of 167.6±1.6 and 167.8±0.4, respectively. There is no indication of isospin mass-splitting. The ratio $(\Sigma_c^{++} + \Sigma_c^{0})/\Lambda_c$ is found to be 0.40±0.29 (<0.74 with 90% confidence). This estimated ratio of Σ_c production rate to Λ_c production rate is too imprecise to deduce any strong conclusion about suppression of $(ud)_1$ diquark relative to $(ud)_0$. The Σ_c^* particles have not been observable in this experiment; why they are not observed needs more attention and further study by physics community.

Future improvements in our knowledge of the Λ_c decay branching fractions, combined with larger data samples on Λ_c production and models such as LUND, WEBBER, and UCLA, can lead to improved understanding of the colorfield dynamics near a heavy quark.

Appendix: Function Averaging

Let's assume that $f(x_1, x_2, \dots x_n)$ is a function of n independent $x_1, x_2, \dots x_n$ variables. If the function f can be represented as

$$f(x_1, x_2, \dots x_n) = \alpha_1(x_1)\, \alpha_2(x_2) \dots \alpha_n(x_n) ;$$

where $\alpha_i(x_i)$ is a continuous function of x_i, then the average of the function f can be evaluated from:

$$\langle f(x_1, x_2, \dots x_n)\rangle = \frac{\langle f\rangle_{x_1} \langle f\rangle_{x_2} \dots \langle f\rangle_{x_n}}{f(x_1^o, x_2^o, \dots x_n^o)^{n-1}} \qquad \text{(A.1)}$$

where $\langle f\rangle_{x_i}$ is the average value of the function f over the variable x_i when the rest of the n-1 variables are fixed at $x_1 = x_1^o, \dots x_{i-1} = x_{i-1}^o, x_{i+1} = x_{i+1}^o, \dots x_n = x_n^o$.

Proof:

$$\langle f(x_1, x_2, \dots x_n)\rangle =$$

$$\langle \alpha_1(x_1)\, \alpha_2(x_2) \dots \alpha_n(x_n)\rangle = \langle \alpha_1(x_1)\rangle \langle \alpha_2(x_2) \dots \alpha_n(x_n)\rangle .$$

If within $\langle \alpha_1(x_1)\rangle$ term, we multiply and divide by the constant coefficient $\alpha_2(x_2^o) \dots \alpha_n(x_n^o)$, then one derives:

$$\left\langle \frac{\alpha_1(x_1)\,\alpha_2(x_2^o)\,\ldots\,\alpha_n(x_n^o)}{\alpha_2(x_2^o)\,\ldots\,\alpha_n(x_n^o)} \right\rangle \left\langle \alpha_2(x_2)\,\ldots\,\alpha_n(x_n) \right\rangle =$$

$$\langle f\rangle_{x_1} \cdot \frac{\langle\alpha_2(x_2)\,\ldots\,\alpha_n(x_n)\rangle}{\alpha_2(x_2^o)\,\ldots\,\alpha_n(x_n^o)} = \langle f\rangle_{x_1} \left\langle \alpha_2(x_2)\,\ldots\,\alpha_n(x_n) \right\rangle \frac{\alpha_1(x_1^o)}{f(x_1^o,\, x_2^o, \ldots\, x_n^o)}.$$

After iterating the same averaging procedure with respect to variable x_2 then for, x_3 and up to variable x_n, then one may derive:

$$= \langle f\rangle_{x_1}\langle f\rangle_{x_2}\,\ldots\,\langle f\rangle_{x_n} \frac{\alpha_1(x_1^o)\alpha_2(x_2^o)\ldots\,\alpha_n(x_n^o)}{(f(x_1^o,\, x_2^o, \ldots\, x_n^o))^n} = \frac{\langle f\rangle_{x_1}\langle f\rangle_{x_2}\ldots\,\langle f\rangle_{x_n}}{f(x_1^o,\, x_2^o, \ldots\, x_n^o)^{n-1}};$$

which proves the Formula A.1.

The averaging algorithm A.1 saves a large number of steps when one tries to numerically estimate the average of the function f. For example, if one numerically estimates the average of function f (which can be represented as $f(x_1, x_2, \ldots x_n) = \alpha_1(x_1)\,\alpha_2(x_2)\,\ldots\,\alpha_n(x_n)$) and uses the algorithm (A.1) and if each variable x_i varies m times within its boundary limits, then the function f may need to be evaluated only nm times. In the case when one resorts to the standard algorithm (see Formula A.2) to average the function f, one may need to estimate the function f as many as m^n times.

$$\langle f(x_1, x_2, \ldots x_n)\rangle = \frac{1}{m^n} \sum_{i_1=1}^{m} \sum_{i_2=1}^{m} \ldots \sum_{i_n=1}^{m} f(x_{i_1}, x_{i_2}, \ldots\ x_{i_n}) \qquad \text{(A.2)}$$